



VADOSE DIAGENETIC DISSOLUTION TEXTURES, CEMENTATION PATTERNS, AND ARAGONITE AND Mg-CALCITE ALTERATION IN THE HOLOCENE ISLA CANCÚN EOLIANITE ARAGONITIC OIDS: MODERN ANALOG FOR ANCIENT OOID-GRAINSTONE PORE NETWORKS

Robert G. Loucks¹ and Kim Patty²

¹*Bureau of Economic Geology, Jackson School of Geosciences, University of Texas at Austin, University Station, Box X, Austin, Texas 78713–8924, U.S.A.*

²*Chesapeake Energy Corporation, P.O. Box 18496, Oklahoma City, Oklahoma 73154–0496, U.S.A.*

ABSTRACT

The Holocene Cancún Eolianite along the eastern shore of Isla Cancún in Yucatán, Mexico, is an excellent natural laboratory for investigating sedimentological and diagenetic processes in a costal carbonate eolian-dune system. The eroded outcrops, comprised of loose ooid sand to lithified ooid grainstone, present well-exposed dune stratification consisting of climbing trans-lent stratification, grainfall laminations, and sandflow cross-stratification. The sediments are comprised of aragonitic ooids that are undergoing extensive early diagenesis in the vadose zone by meteoric water. Different parts of the eolianite have achieved various stages of diagenesis, which allows the observation and understanding of the progression of aragonite ooid sand/grainstone stabilization. Dissolution of the unstable aragonite and Mg-calcite nuclei creates oomoldic pores, and the generated calcium carbonate is reprecipitated as very fine- to fine-crystalline equant calcite in interparticle pores. In ooid cortices, aragonite needles undergo dissolution by separating into nanoballs. No cement is being reprecipitated in the dissolving nuclei for lack of suitable nucleation sites. The vadose zone of the Cancún Eolianite is a closed system relative to conservation of calcium carbonate. The amount of dissolution of aragonite and Mg-calcite approximates the amount of very fine- to fine-crystalline equant calcite cement in the interparticle pore space. The early pore network has many similarities to ancient pore networks in ooid grainstones, such as cement-reduced interparticle pores, cortex-dissolution-band pores, oomoldic pores, and abundant nano- to micropores in altered ooids. Concepts derived from investigating the Cancún Eolianite can be applied to understanding how ancient ooid-reservoir pore networks formed and evolved.

INTRODUCTION

A well-exposed Holocene oolitic eolianite (Cancún Eolianite, 1400 to 3800 yr old) occurs along the eastern shore of Isla Cancún in Yucatán, Mexico (Figs. 1 and 2). Because of its early initial lithification in the vadose zone and erosion by storms, it exposes exceptional three-dimensional (3D) outcrops where bedding is well displayed. The eolianite shows early stages of diagenesis and pore evolution. These outcrops provide a natural laboratory where sedimentological and carbonate diagenetic processes can be investigated.

Ooid grainstones in the ancient record form many economic carbonate reservoirs whose environments of deposition, burial paragenesis, and associated pore networks have been investigated (e.g., Benson and Mancini, 1982; Cantrell, 2006; Honarmand and Amini, 2012; Esrafil-Dizaji and Rahimpour-Bonab, 2014); however, few detailed examples of aragonite ooid diagenesis are available from Holocene deposits, and these studies mainly addressed the destruction and formation of macropores and diagenetic geochemical processes (e.g., Ward, 1975; Picha, 1978; Halley and Harris, 1979; Longman et al., 1983; Strasser and Davaud, 1986; Budd, 1988; Budd and Land, 1990; McLaren and Gardner, 2004). It is important to understand not only the macropores but also the micropores that form in ooids. In ancient ooid-grainstone reservoirs, micropores in the ooids affect production, water saturation, and capillary-pressure characteristics (Keith and Pittman, 1983), especially in dual-pore reservoirs comprised of macropores and micropores.

Copyright © 2017. Gulf Coast Association of Geological Societies. All rights reserved.

Manuscript received March 2, 2017; revised manuscript received May 10, 2017; manuscript accepted May 26, 2017.

GCAGS Journal, v. 6 (2017), p. 1–20.

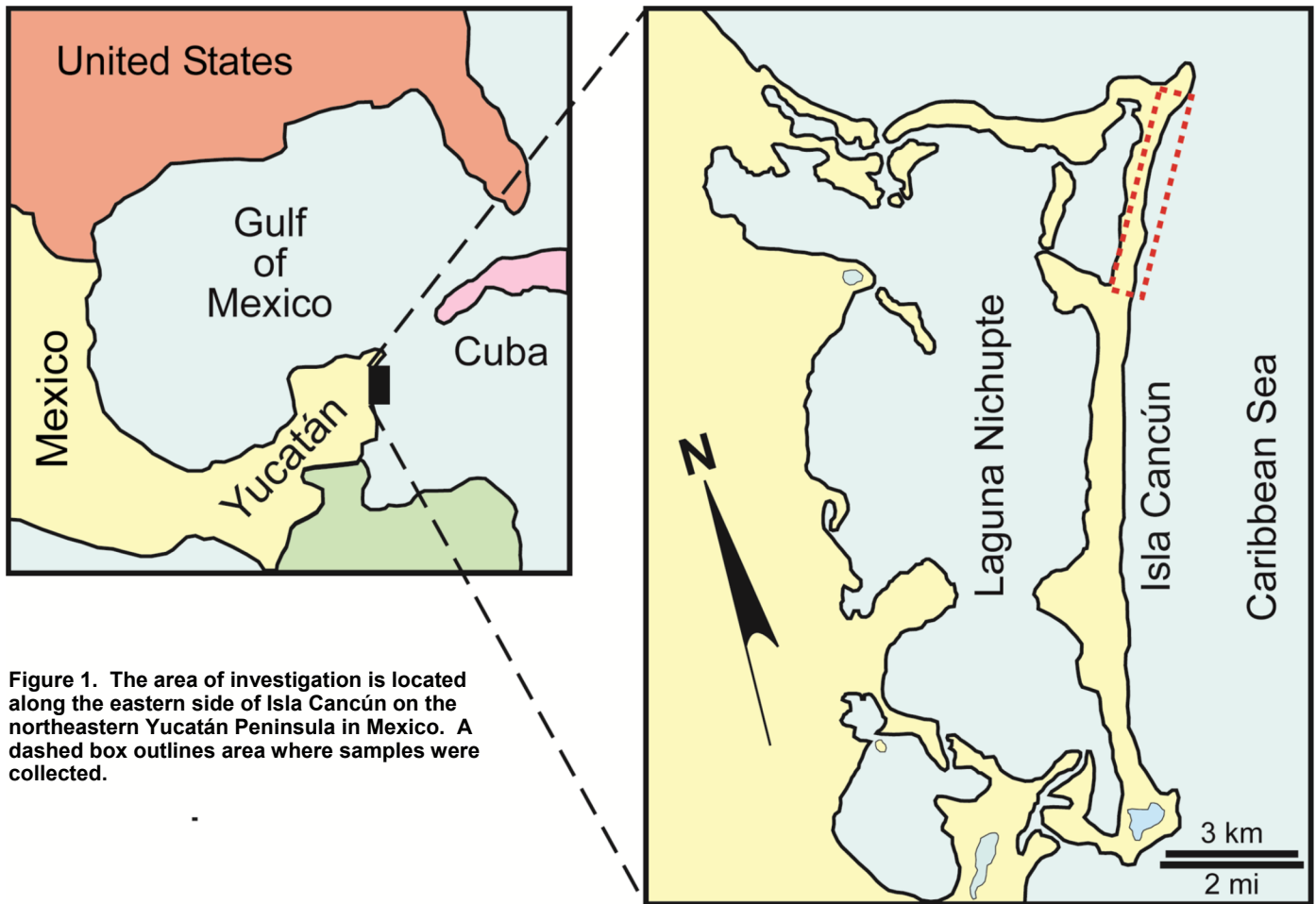


Figure 1. The area of investigation is located along the eastern side of Isla Cancún on the northeastern Yucatán Peninsula in Mexico. A dashed box outlines area where samples were collected.

The objectives of this investigation are to: (1) provide a short description of stratification types within the Cancún Eolianite; (2) outline stages of diagenesis including mineralogical transformations, cementation, and dissolution features; (3) summarize primary interparticle porosity destruction and secondary oomoldic porosity formation; (4) describe alteration of aragonite needles in the ooid nuclei and cortex; (5) propose a mechanism that allows precipitation of cement in interparticle pores, while oomoldic pores remain cement free; (6) discuss whether the vadose zone operates as an open or closed system with respect to the dissolution and precipitation of calcium carbonate; and (7) discuss preservation potential of carbonate eolian dunes. Addressing these objectives will aid in understanding the development of complex dual-pore networks (micro- and macropores) in ooid grainstones, the origin of oomoldic-rich grainstones, and the probability of the preservation of coastal eolian carbonate dunes.

DATA AND METHODS

Eolianite outcrops were described in detail for bedding types; lateral and vertical changes; and other features such as storm truncation, bioturbation, and caliche formation. A detailed sedimentological investigation of these outcrops was published by Ward (1975) and Loucks and Ward (2001). Hand samples from several locations, mainly from the northern third of Isla Cancún, were collected. One set of samples that was collected immediately north of the Hilton Hotel was from an excavation for a new hotel. That site is now covered. The samples were slabbed to identify mesoscale depositional and biogenic features. Fifty-five thin sections impregnated with blue-dyed epoxy were

prepared, analyzed, and photographed for texture, fabric, biota, diagenetic features, and pore types. The blue epoxy emphasizes pores and ensures recognition of thin-section plucking of material. Thirty of the thin sections were point-counted for cement and pore types. Per thin section, 1000 points were counted, providing an accurate estimate for amount of cement, its location, and macropore types. Mineralogy was defined by X-ray diffraction (XRD) analysis by ARCO Oil and Gas Company (bought by BP). Because many of the diagenetic features can only be resolved at the nano- to microscale, samples were observed using an FEI Nova NanoSEM 430 at the University of Texas at Austin. Use of this field-emission scanning electron microscope (FESEM) equipped with in-lens secondary electron detectors provided greatly enhanced detail of nanometer-scale features. Lower accelerating voltages (10–15 kV) were generally used on these samples to prevent beam damage, and working distances were 3 to 7 mm.

Four types of samples were viewed with the FESEM: rock chips, polished thin sections, etched thin-section stubs (pore casts), and Ar-ion milled samples. Rock chips allow the 3D aspect of the material to be observed, and broken ooids within the chips provide observation of ooid-internal structure. The crystal morphology of the calcite cement is readily apparent, and the nano- and micropores are observable. Polished thin sections permit the viewing of a large area in a two-dimensional plane. Because the thin sections are impregnated with epoxy, many of the micron-sized features are obscured; however, high-contrast backscatter images provide excellent maps of micro- to macropore networks. Pore casts were prepared from impregnated thin-section stubs by etching the stub with HCl. To prepare the stubs, they were submerged in epoxy and put under a vacuum

Holocene	Blanca Eolianite	~1400 years BP to present
	Cancún Eolianite	~3800 to 1400 years BP
Pleistocene	Pleistocene eolianites	

Figure 2. General stratigraphic section of eolianites on Isla Cancún. Age dates are from Loucks and Ward (2001).

for 24 hr and then subjected to a pressure of 2000 psi (14 MPa) to insure that the epoxy filled the majority of pores. After etching, the material (epoxy) that stands in relief in a pure limestone represents the pore network. Ar-ion milled samples (see Loucks et al., 2009, for discussion of description and preparation of Ar-ion milled samples) are excellent for observing a flat surface without any irregularities related to differential hardness. These samples also allow some degree of 3D viewing because they are not impregnated with epoxy. Porosity measurements were performed on six core plugs (1 in [2.5 cm] diameter) by Core Laboratories.

GEOLOGIC SETTING

Isla Cancún lies off the northeastern coast of the Yucatán Peninsula of Mexico (Fig. 1). The island, which is approximately 8 mi (13 km) long and 0.6 mi (0.9 km) wide, is connected to the mainland by two tombolos that extend landward from the island's northern and southern rocky points. On the Caribbean side of Isla Cancún, the beach passes a short distance landward into a 56 ft (17 m) high ridge of eolianites comprised of aragonitic ooids (Fig. 3). The Cancún Eolianite age is between 1400 and 3800 years BP based on radiocarbon dating (Loucks and Ward, 2001). Another study (McLaren and Gardner, 2000) dated the eolianite as between 2500 and 4000 years BP. Considering the complexity of dune growth and erosion, these ranges of dates are in fair agreement, positioning the Cancún Eolianite as being deposited during the latest part of the Holocene sea-level rise (McLaren and Gardner, 2000). Ward (1997) described older Pleistocene eolianites on the backside of Isla Cancún, and the younger Blanca Eolianite (Fig. 2) along the middle seaward side of the island (Ward, 1975, 1997; Ward and Brady, 1979).

Prevailing winds in the area are northeasterly to easterly in winter and southeasterly to easterly in summer (Ward, 1975, 1997). Spring tides are approximately 2 ft (0.6 m) and neap tides are 1 ft (0.3 m). Rainfall in northeastern Yucatán averages about 50 in/yr (130 cm/yr) (subtropical), with the rainy season extending from May to September (Current Results Publishing Ltd., 2017). A number of hurricanes have crossed northeastern Yucatán, with the second strongest in Mexico's recorded history being Hurricane Gilbert, which battered the coast in 1988 with winds of over 185 mph (300 kmph; Category 5 hurricane) and a storm surge of over 21 ft (7 m).

DESCRIPTION OF THE CANCÚN EOLIANITE

Grain, Sediment, and Rock Types

The Cancún Eolianite is comprised of ooid-coated grains (Fig. 3). Nuclei are predominantly fragments of aragonitic *Halimeda* (green algae) and Mg–calcite *Goniolithon* (red algae) as well as lesser amounts of peloids, foraminifers, mollusks, and lithoclasts (Fig. 3A). Oolitic coatings (cortex) range in thickness from less than 10 microns to over 50 microns (Fig. 3). Individual layers of aragonite needles in the cortex show both tangential layering and relatively random layering (Figs. 4A and 4B). The more random layers show relatively looser packing. The tangential layering produces a pseudouniaxial cross under cross-polarized light (Fig. 4D). Common features in the cortex are microborings by fungi or algae (Fig. 3D). Cements comprised of Mg–calcite are precipitated around some of the microborings, similar to Mg–calcite cementation described by Winland (1968).

The sediments are well sorted, making it difficult to recognize internal bedding features such as fining-upward and coarsening-upward grain fabrics in thin sections. The loose sand in the eolian dunes would be classified as well-sorted oolitic lime sand, whereas the lithified sediments would be classified as well-sorted ooid lime grainstone.

XRD analyses (Fig. 5) show that loose ooids (framework grains) from the modern shoreface are predominantly aragonite (91–94%), with some Mg–calcite (3–7%) and calcite (2–3%). The Holocene Cancún Eolianite displays a range of mineralogies from near those of modern shoreface sediments to mineralogies of up to 35% calcite with no Mg–calcite (Fig. 5). This mineralogical trend reflects increasing diagenesis by meteoric waters (Land, 1967). Unstable Mg–calcite and aragonite are undergoing dissolution and reprecipitation to calcite.

Some samples, on the basis of XRD analysis, show a quartz content up to 2.8%, with an average of all samples of 0.9%. No quartz grains could be identified in thin section, but micron-sized (<2 microns) rounded quartz grains could be seen with FESEM imaging. The origin of this micron-sized quartz is interpreted as dust from a distance source. A few micron-sized clay flakes were also noted with FESEM imaging; these particles are also probably dust.

Eolian Stratification Types

Stratification types observed in the carbonate Cancún Eolianite coastal dunes have been described by Loucks and Ward (2001). Their observations of stratification types parallel the observations by Hunter (1977) for siliciclastic coastal dunes. The eolianite is characterized by numerous bounding surfaces, which are discussed in detail in Loucks and Ward (2001). Longman et al. (1983) also investigated some prominent surfaces in the Cancún Eolianite. The two major causes of the truncated surfaces are erosion during major storms and by dunes changing direction of migration. A modified beach-to-dune depositional model published by Loucks and Ward (2001) is shown in Figure 6.

The most common stratification type in the Cancún Eolianite is climbing translant stratification produced by wind ripples migrating across the dune (Figs. 6 and 7A) (Hunter, 1977). Wind ripples—which produced thin (1 to 2 mm), isopachous laminae on low-angle slopes—can occur on both the windward and leeward sides of the dune (e.g., Clemmensen and Abrahamsen, 1983; Hunter, 1993). In other climbing-translant stratification deposits, laminae display inversely graded bedding, which is, however, uncommon in the Cancún Eolianite because of the well sorting of the ooids.

Grainfall laminations (Figs. 6, 7B, and 7C) developed on the leeward side of dunes, where separation flow occurs and airborne grains fall onto the foreset slope (Hunter, 1977). High-angle (14 to 30 degrees), relatively uniform but diffuse laminae form.

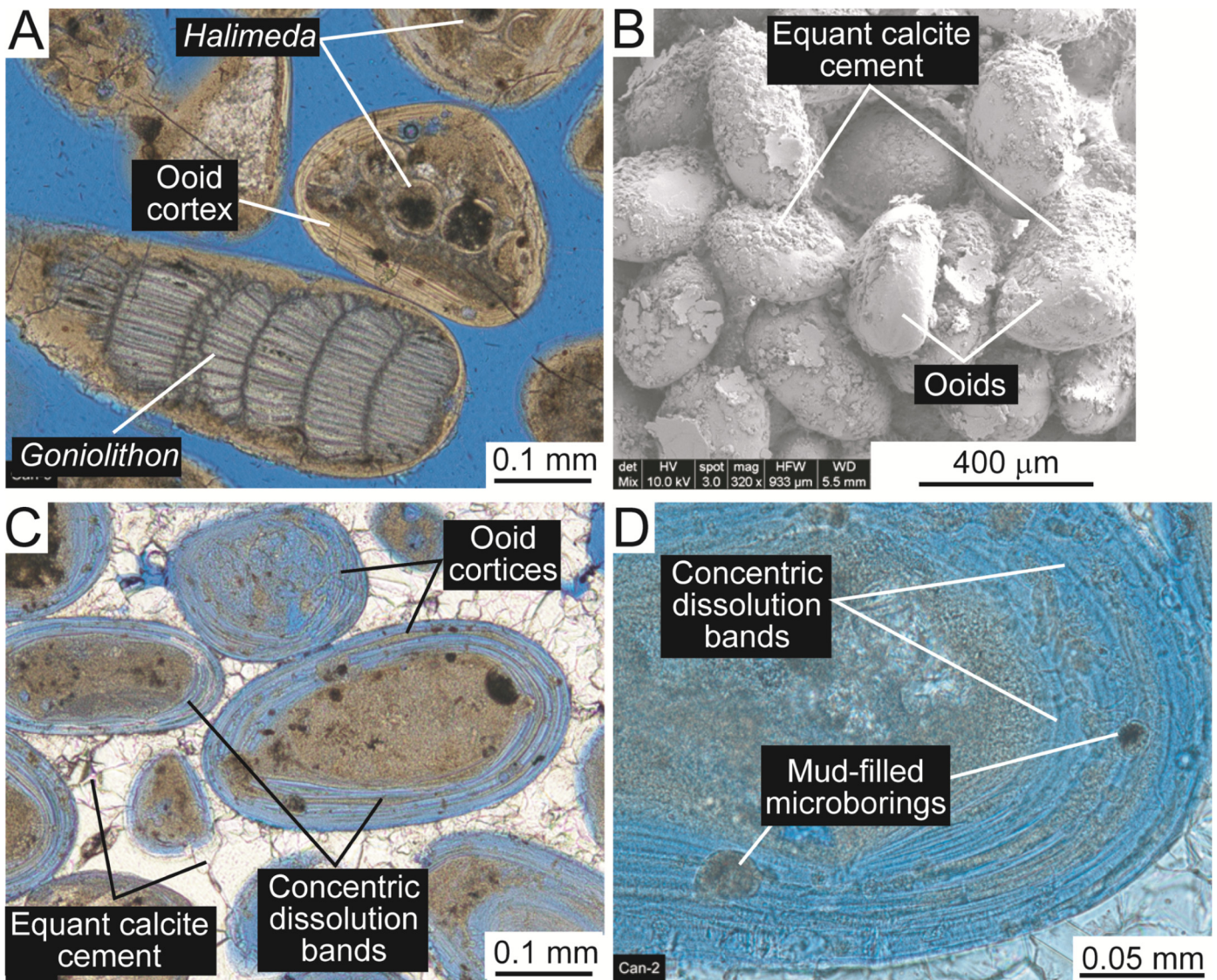


Figure 3. Examples of Cancún ooids. (A) Thin section of unaltered ooids. *Halimeda* and *Goniolithon* are the nuclei. (B) SEM images of ooids with a light coating of equant calcite cement. (C) Thin section showing ooids with thick cortices and well-developed dissolution bands. (D) Close-up of thin-section photomicrograph of concentric dissolution bands.

Thickness of the laminae varies and is related to the duration of exposure to the wind (Fryberger and Schenk, 1981).

Sandflow cross-stratification is generated by avalanching of tongue- and cone-shaped masses of noncohesive sand down foreset slip faces (Figs. 6, 7C, and 7D), whose inclination is at the angle of repose (30 to 32 degrees) (Hunter, 1977; Loucks and Ward, 2001). Sandflows—which have sharp contacts, are lenticular, and have distinct pinch-outs, or toes—are up to 1.2 in (3 cm) thick and commonly appear dark relative to associated grainfall laminae.

Stratification is well preserved in the dunes except for a few zones bioturbated by roots. In the modern dunes (Blanca Eolianite), vegetation is predominantly on the leeward side and includes shrubs, trees, scrub palms, cactus, and grasses (Ward, 1975). In the Cancún Eolianite, most rhizoliths are root molds preserved as uncemented tubular holes. A few animal burrows and footprints were also noted (Loucks and Ward, 2001).

Diagenesis

Early Paragenesis of the Cancún Eolianite

Even though the Cancún Eolianite is relatively young, portions of the dune system have undergone extensive diagenesis.

The degree of diagenesis within the dunes showed no recognizable pattern and probably is related to permeable pathways. The underlying cause of this diagenesis is the high abundance of unstable minerals (aragonite and Mg-calcite) being subjected to meteoric waters in the vadose zone. In this diagenetic environment, aragonite and Mg-calcite dissolve and reprecipitate to form calcite (e.g., Friedman, 1964; Land, 1967, 1970; Matthews, 1967, 1968; Gavish and Friedman, 1969; Steinen and Matthews, 1973; Ward, 1975). As mentioned in the “Introduction,” the Cancún Eolianite is a natural laboratory for studying the processes and products of early ooid paragenesis.

Meteoric water is the dominant fluid that affects allochems in the dunes. It has been well documented that aragonite and Mg-calcite are unstable in meteoric water (e.g., Land, 1967). The dunes are also subjected to sea spray from onshore wind and to flooding of marine waters during large storms (hurricanes); however, these fluids should not promote diagenesis because aragonite and Mg-calcite are stable in these fluids. McLaren (1995) and McLaren and Gardner (2000, 2004) suggested that sea spray could be a partial source of fluids for cementation and dissolution; however, this present study considers sea spray to be a limited source of fluid that would only affect the surface of the dunes. Also, residence time of these fluids would be so limited

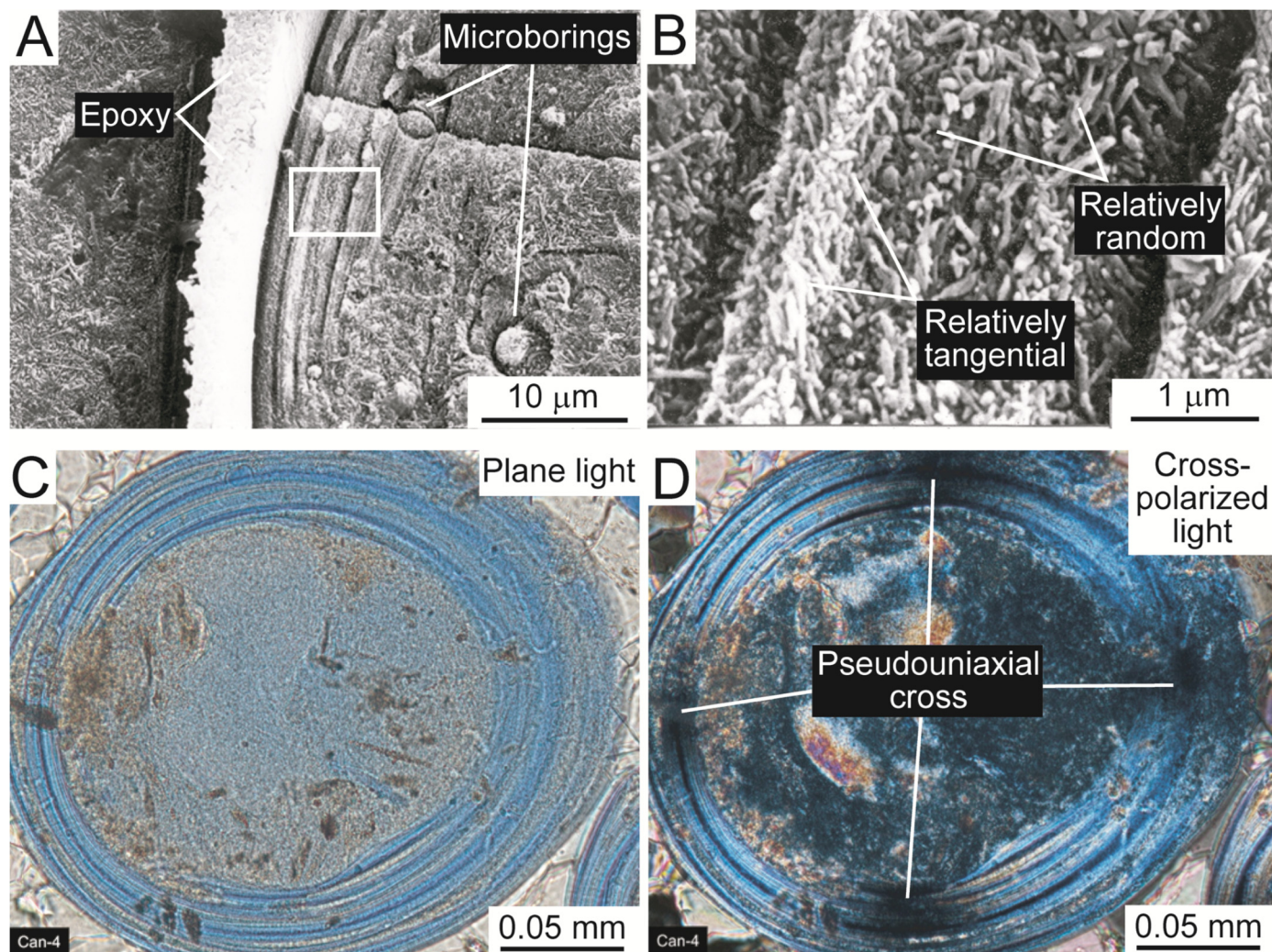


Figure 4. Packing arrangement of aragonite needles in ooid cortex. (A) Pore-cast SEM image of ooid cortex showing area of enlargement in B. (B) Pore-cast SEM image showing cortex bands. Some bands have a more tangential packing arrangement than other bands. The more random or looser packed bands appear to have more porosity between needles and may allow more through-going fluid movement. (C) Thin-section image displaying concentric dissolution pores in ooid cortex. Partly dissolved aragonite *Halimeda* nuclei are highly microporous. (D) Same as C but under cross-polarized light. Because tangential layered cortex bands are preserved, a strong pseudouniaxial cross appears under cross-polarized light.

as to not effectively accomplish any alteration. The samples used in the present investigation were all collected away from the surface of the dunes and out of reach of any sea-spray effect. However, several samples do display an amorphous, several-micron rim rich in Si, Na, Mg, and Al that may be a bacterial biofilm related to sea spray (discussed later in the section on “Amorphous Rims”).

Dissolution

Ooid Nuclei Dissolution

The most common ooid nuclei are comprised of aragonite (*Halimeda*) and Mg–calcite (*Goniolithon*) (Fig. 3A), which are unstable in meteoric waters. Both grain types in the Cancún Eolianite are seen at different stages of dissolution, ranging from partial-grain dissolution to complete dissolution (moldic pores) (Fig. 8). It is interesting that in the Cancún Eolianite, red algae undergo complete dissolution, while in other formations they commonly convert to microrhombic calcite and preserve the fabric of the original grain (Loucks et al., 2013).

The progressive dissolution of aragonite and Mg–calcite is well displayed in Figure 9, where the percent of aragonite and Mg–calcite derived from XRD analysis is plotted relative to cal-

cite. The majority of calcite is present in the form of very fine-to fine-crystalline equant crystals that are related to cementation in the vadose zone. The increase in percentage of calcite is an indicator of the advancement of or a proxy for diagenesis. Therefore, in Figure 9, as calcite increases, aragonite and Mg–calcite decrease. At approximately 20% calcite, all of the Mg–calcite has dissolved and reprecipitated as calcite. One might conclude that Mg–calcite is more unstable than aragonite and that is why it disappears first. But actually, by the time 3 to 5% of Mg–calcite has disappeared, 13% of aragonite has already disappeared. Oomoldic pores are generally free of calcite cement, suggesting that oomoldic pores have a high potential for preservation.

Ooid Cortex Dissolution

All of the ooid cortices are comprised of aragonite needles (Figs. 4B and 10). Dissolution within the cortices appears as multiple distinct bands (Figs. 3C, 3D, 4A, 4C, and 8). Budd (1988) and Budd and Land (1990) also noted these dissolution bands in Holocene ooids from Schooner Cays, Bahamas (see their figure 5F). The distinct bands cannot be related to differences in mineralogy because the complete cortex is comprised of aragonite needles. To help understand the reason for the differ-

Figure 5. Mineralogical contents of Cancún ooids and eolianites plotted in a ternary diagram based on XRD data.

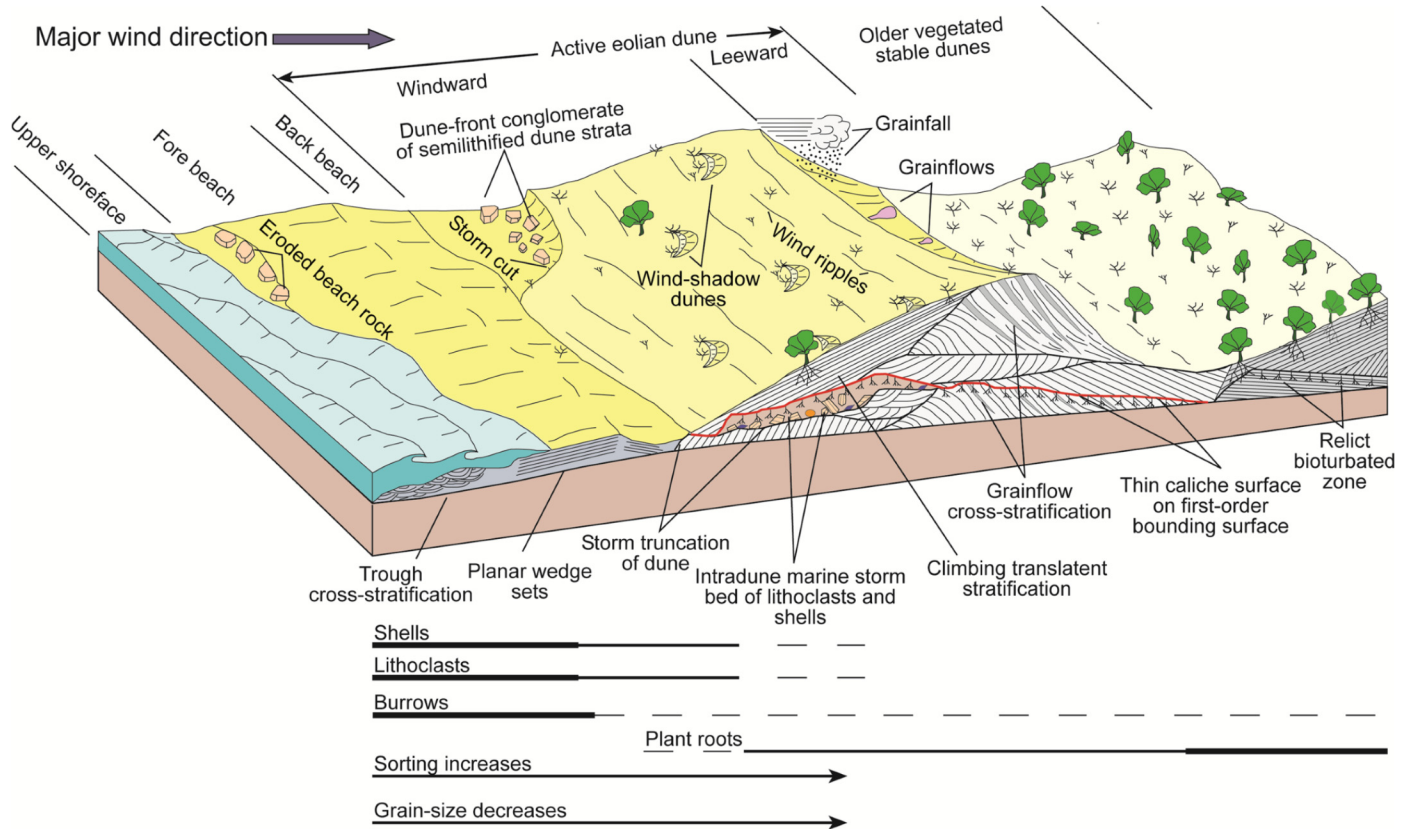
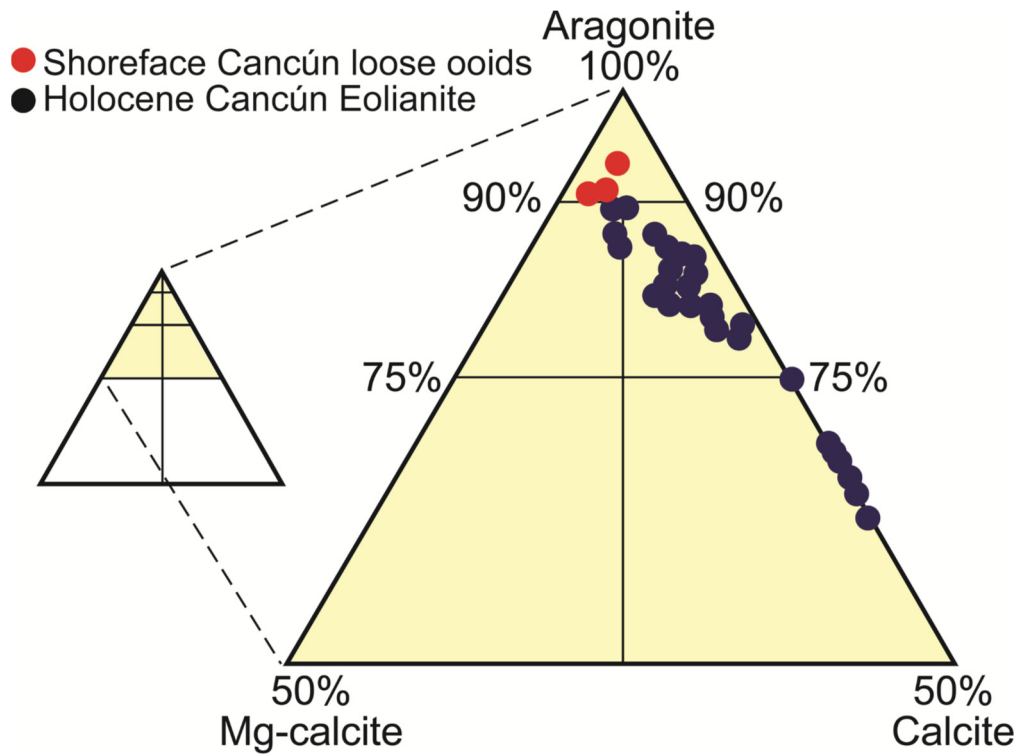


Figure 6. Depositional model for beach and eolian dune environments (modified after Loucks and Ward, 2001).

ential dissolution rates, we conducted an experiment where a polished face of a weakly impregnated modern ooid sand sample was etched in very weak HCl for a few seconds (Figs. 4A and 4B). The sample was then imaged using an SEM to observe any differences in dissolution. As Figure 4B shows, the different cortex bands show different amounts of dissolution. In the bands

showing the least dissolution, the aragonite needles appear to be the most tangentially packed and parallel to the nuclei, whereas the bands showing more dissolution are more randomly packed. In the randomly packed bands, porosity appears to be higher, suggesting that the bands with higher porosity would allow more through-going fluid flow, thus promoting more dissolution.

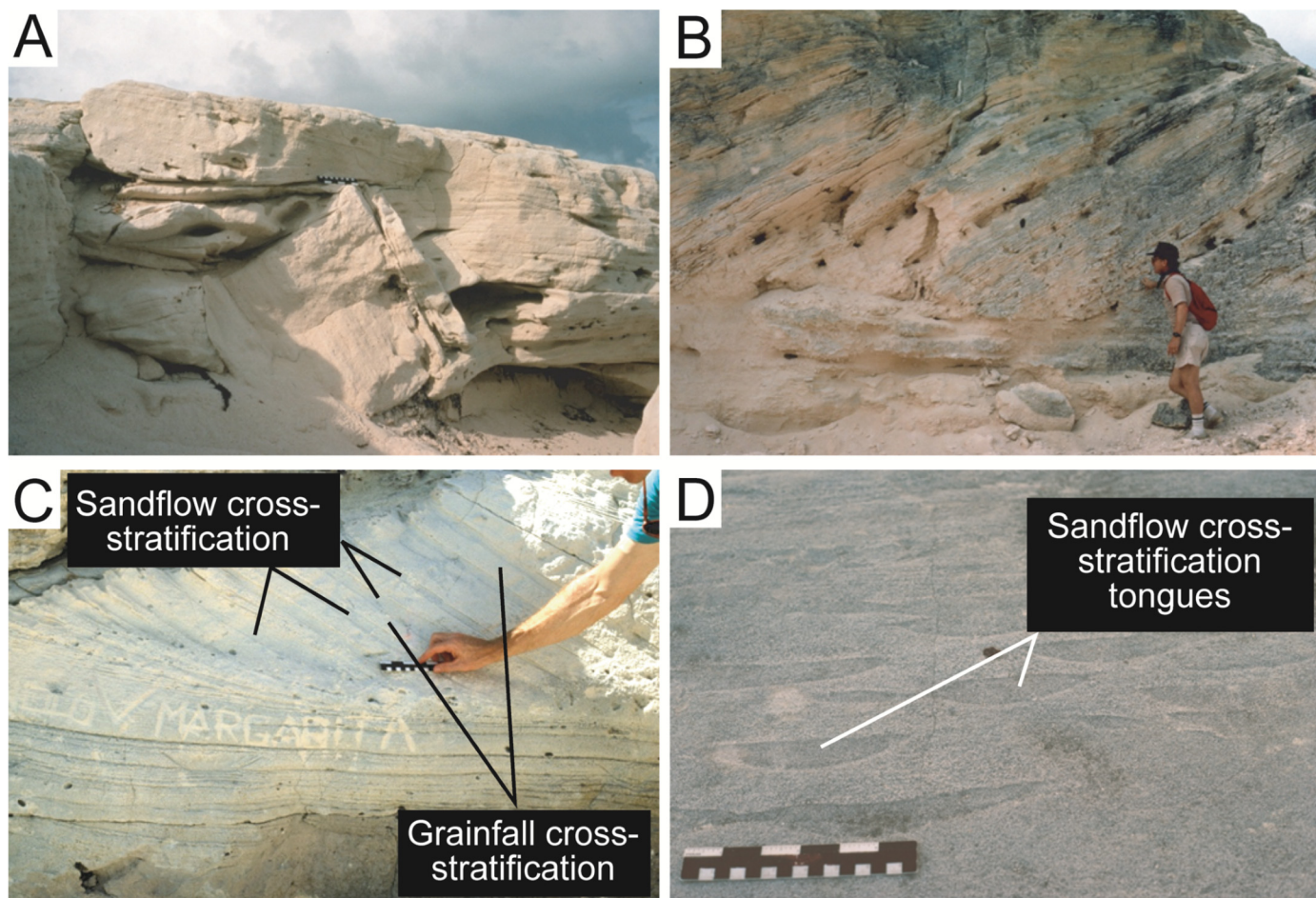


Figure 7. Examples of stratification types in the Cancún Eolianite. (A) Outcrop of the Cancún Eolianite comprised mainly of climbing translant stratification sets. The climbing translant stratification buried a semilithified block of eolianite produced by storm processes. Seaward is to the right. Scale is 6 in (15 cm). (B) Outcrop of the Cancún Eolianite comprised of a thick set of grainfall lamination downlapping onto a bed of climbing translant stratification. Seaward is to the right. (C) Sandflow cross-stratification (high-angle, darker shaded, recessed layers) and grainfall lamination (high-angle, lighter shaded, raised layers) downlapping onto climbing translant stratification. The dune slipface is truncated, and only the lower part of the sandflow cross-stratification and grainfall lamination are preserved. Scale is 6 in (15 cm). (D) Plan view of sandflow cross-stratification displaying simple lens with erosional convex down base and curved top. Scale is 6 in (15 cm).

Under cross-polarized light, preserved cortex bands in the Cancún Eolianite display distinct pseudouniaxial crosses (Figs. 4C and 4D). A pseudouniaxial cross is a function of the aragonite needles being oriented parallel to the grain nuclei surface, which is evidence that the preserved cortex bands are comprised of the layers that have parallel packed aragonite needles tangential to the ooid. Some preserved cortex bands may be related to having been converted to nanocrystalline calcite. However, because of the very fine size of the crystals, it is not possible to separate degrading aragonite nanoballs (nano-sized calcium-carbonate particles) from calcite nanoballs. Crystal habit can help because some degraded aragonite is still needle shaped and some calcite cement is rhombohedral.

Aragonite Needle Dissolution

The above discussion of nuclei and cortex dissolution was generally at the macroscale. The actual process of dissolution is at the microscale of the aragonite crystals. The stages of aragonite dissolution were identified using the FESEM (Fig. 10). Because Mg–calcite (allochems comprised of Mg–calcite rods) is only a few percent of the rock volume, it was difficult to recognize it with the FESEM, so it was not investigated. However, comparing the results from this study on dissolution of aragonite

needles to other results on dissolution of Mg–calcite rods (Budd and Hiatt, 1993; Macintyre and Reid, 1998; Hover et al., 2001; Loucks et al., 2013), it appears that the dissolution processes for both aragonite and Mg–calcite are similar. The stages of aragonite dissolution are summarized diagrammatically in Figure 10E.

In the Cancún ooids, pristine aragonite crystals have a needle shape with sharp and straight edges (~1 micron long and 0.1 micron wide) (Figs. 10A and 10E). As dissolution begins, crystal faces become irregular, indicating initiation of separation into nanoballs less than 100 nm wide (Figs. 10B and 10E). With further dissolution, the separation into nanoballs is more prominent (Figs. 10C and 10E). At this stage, there is an approximately even mixture of altered needles and nanoballs. Figures 10D and 10E show the original aragonite needle mesh comprised predominantly of nanoballs and some irregular needles.

There was no way to document that the nanoballs are still aragonite and not calcite. The energy dispersive spectroscopy (EDS) analysis on the FESEM could not detect the differences in Sr between aragonite (high Sr) and calcite (low Sr), which would have helped to differentiate the two minerals. It is assumed that the composition of the nanoballs is still aragonite because the nanoballs have rounded edges and generally display no crystal faces that would be evidence of initial calcite crystallization. However, one sample (Fig. 10F) does appear to show some crys-

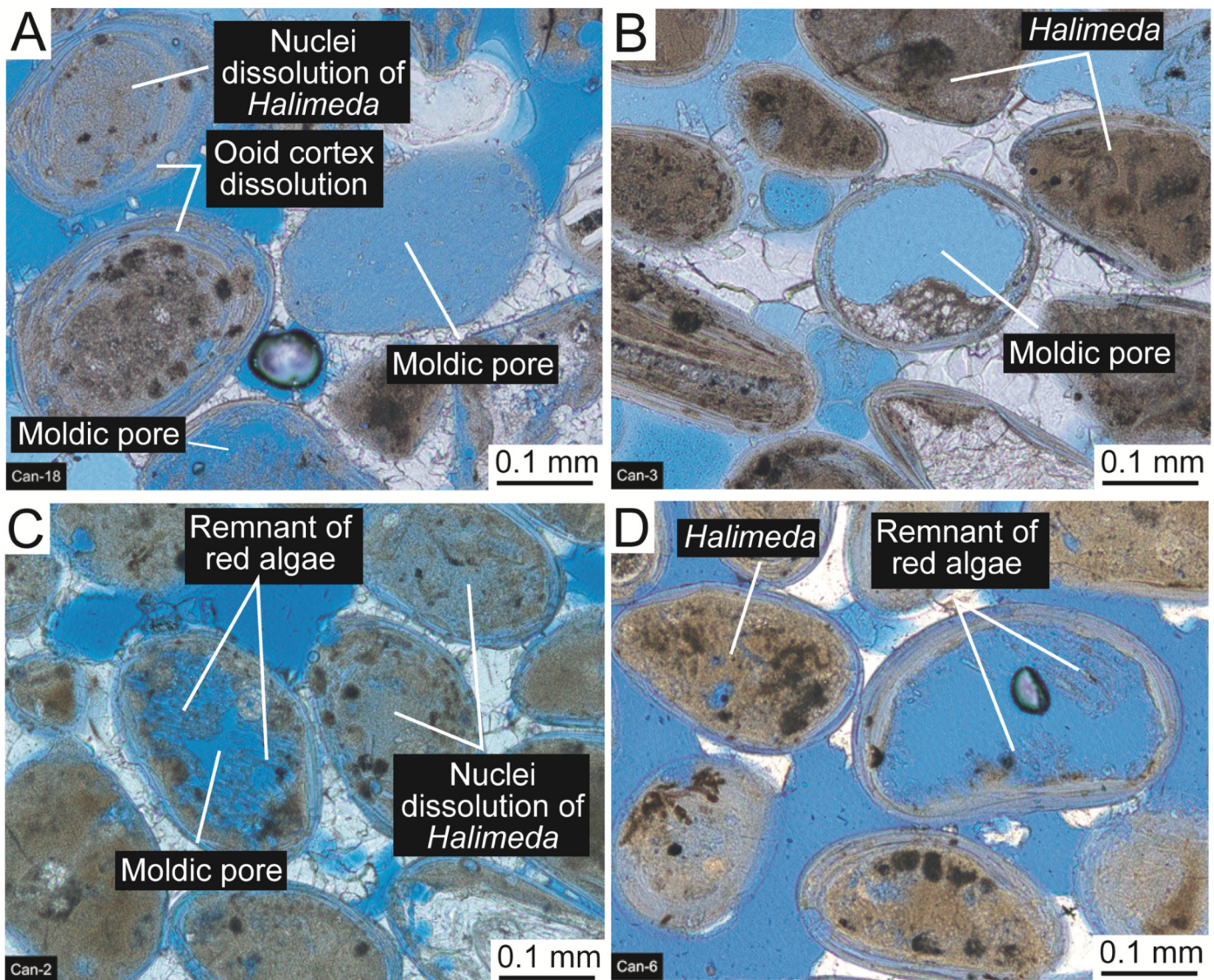


Figure 8. Examples of development of moldic pores. (A) Moldic pores after *Halimeda* dissolution. The central moldic pore has flecks of aragonite remaining. At bottom of photomicrograph is a moldic pore in the middle stage of development. Example of meniscus and interparticle pore-fill center calcite cement. (B) Open moldic pore surrounded by equant calcite cement. (C) Moldic pore is developing as red algae is dissolved. Pore is partly surrounded by equant calcite cement. Several *Halimeda* nuclei are in the process of dissolving. (D) Moldic pore after red algae dissolution. Fragments of red algae still remain. Ooids are cemented by meniscus calcite cement.

tal facies on nano-sized rhombs, and the aragonite crystals may be showing signs of welding (Fig. 10F). Therefore, this sample may be displaying early signs of calcite cementation. Also, the sample shown in Figures 11C and 10D may be undergoing early calcite conversion. Some of the cortex layers show aragonite needles in an advanced stage of alteration. Some layers appear welded, with no evidence of aragonite needles preserved; these could be incipient calcite-cemented layers.

In the Cancún Eolianite, aragonite is documented to dissolve by separating into nanoballs. As suggested in Figure 9, the aragonite nanoballs may continue to dissolve and contribute calcium carbonate to the formation of calcite crystals in the interparticle pore spaces.

Cementation

Cementation Associated with Microborings

As mentioned earlier, a common feature in the cortex is fungi and algal microborings (Fig. 11A). Mg-calcite cements,

which can be associated with these microborings as described by Winland (1968), are the product of precipitation in the chemical microenvironment created by the fungi and algae. The calcite crystals outlining microborings in the Cancún ooids (Fig. 11B) are aphanitic to very fine crystalline. FESEM EDS analysis indicates that the cements are Mg enriched. The calcite crystals related to microborings in the ooid cortex may be important in providing nucleation sites on the outside of the ooid for the initiation of calcite cement.

Cementation within the Cortex

In general, calcite is not precipitating in the cortices of the ooids; however, some rare calcite cementation was observed in the aragonitic cortex (Figs. 11C and 11D). The calcite crystals are several microns in size. In Figure 11D, they can be seen growing around bulbous aragonite crystals and nanoballs. Another example shown in Figures 12C and 12D displays possible calcite-cemented cortex bands, but because of the small size of

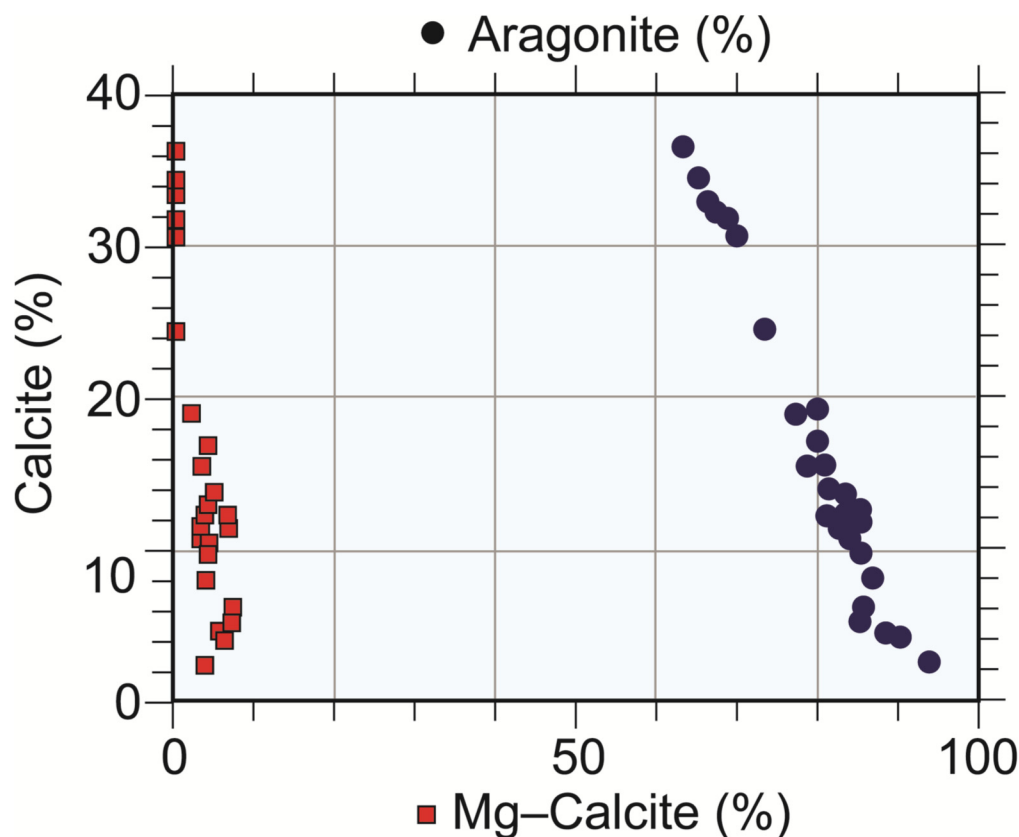


Figure 9. Scattergram based on XRD analysis showing the decrease in aragonite and Mg–calcite as calcite increases. This is evidence that the dissolution of aragonite and Mg–calcite supplies calcium carbonate to form calcite vadose cements. Note that aragonite is dissolving faster than Mg–calcite.

the crystals in the bands mineralogical identification cannot be certain.

Pore-Fill Meniscus Cement

Pore-filling meniscus cement (Dunham, 1971) is common in the interparticle pores. It occurs as very fine- to fine-crystalline, blocky to steep rhombohedra of calcite (Figs. 8D, 13A, and 13B). Some of the cement is Mg enriched, as indicated by FESEM EDS analysis. As the term meniscus implies, the cement is located at grain contacts where vadose water clung between grains. The precipitation of meniscus cement initiated the lithification of the ooid sands.

Grain-Coating Cement

Grain-coating calcite cement occurs as scattered equant anhedral rhombic crystals on the surface of the grains away from the meniscus cement (Figs. 11C and 13B). Crystal sizes range from less than a micron to 30 microns. Many of the crystals are isolated from their neighbors, but some crystals are coalescing. This is an early stage of calcite cementation; as cementation proceeds, the crystals will form into rim cements (Fig. 3B). It is interesting to note that these crystals can be seen only with the aid of the FESEM. In thin section (Fig. 8D), many of the crystals are too small to be resolved.

Interparticle Pore-Fill Center Cement

As diagenesis proceeds, very fine- to fine-crystalline equant calcite precipitates in parts of interparticle pores other than just at grain contacts (meniscus cement) (Figs. 3C, 8B, 8C, 13C, and 13D). In thin section, pores in any one area may be nearly cemented, but at the scale of the whole thin section it can be seen that these cemented areas are domains of enhanced cementation. That this equant calcite cement is precipitated only in interparticle, not moldic, pores will be addressed in the “Discussion” sec-

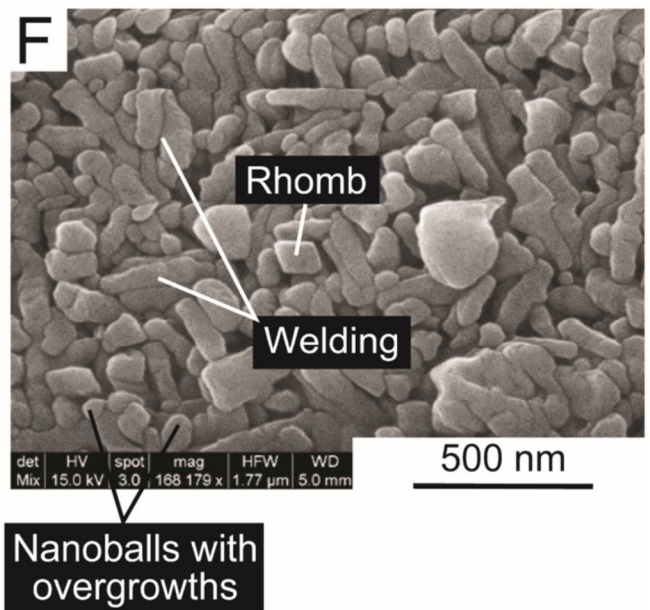
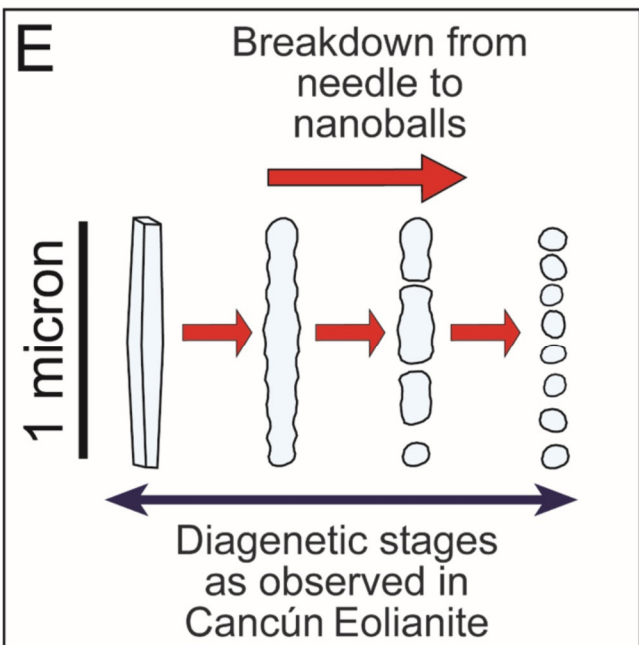
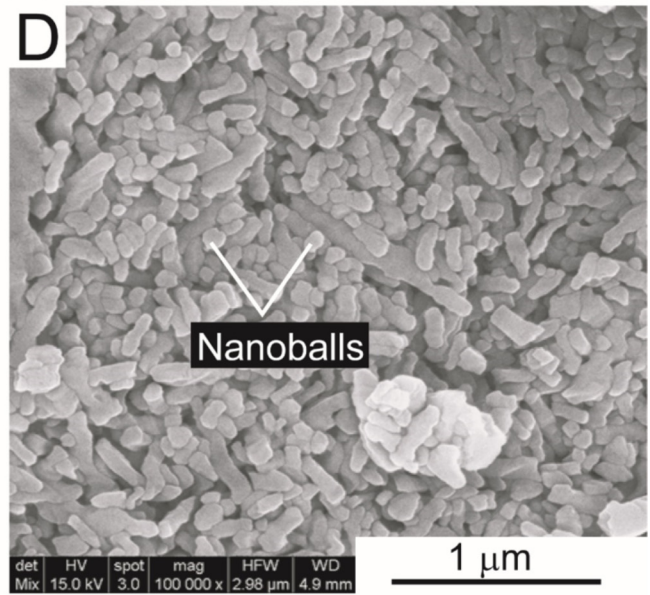
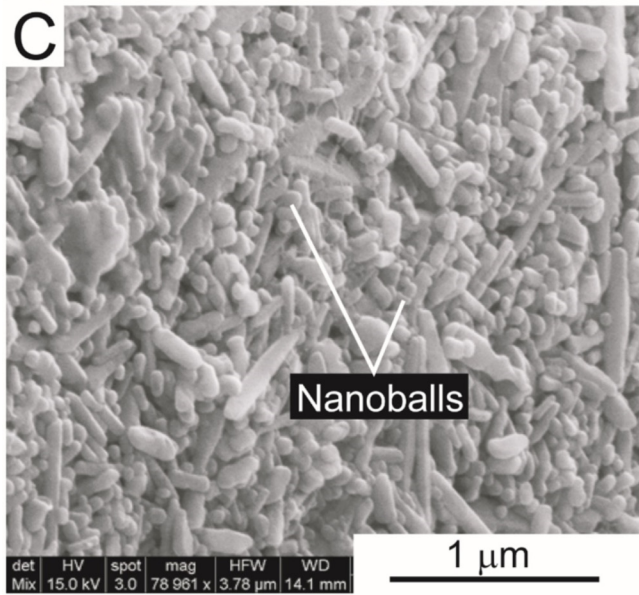
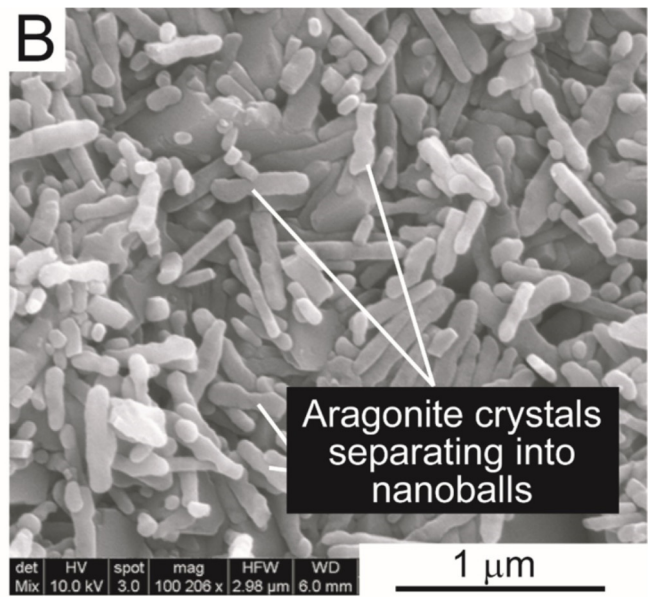
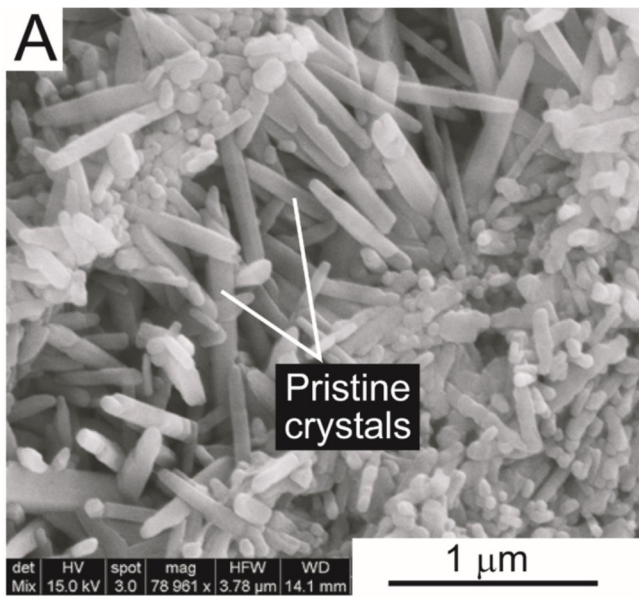
tion. In many ancient limestones, the interparticle pore fill shows a gradation in crystal size toward the center of the pore. In the Cancún Eolianite, this gradation is not very obvious. Also, as the vadose interparticle pores are filled, the remaining pores become rounded (Fig. 13C), which reflects the coalescing of meniscus cement patches. This rounding is not preserved as cementation proceeds.

Amorphous Rims

Some samples display a thin, amorphous coating, or rims, comprised of Si, Na, Mg, Ca, and Al, as indicated by EDS analysis on the FESEM (Fig. 12E). The rims are from 1 to 3 microns thick and coat the whole grain (Fig. 12A); in three dimensions, parts of the coating have bulbous structures (Figs. 12A–12C). Figure 12B is an Ar-ion milled cut through several of these bulbous structures. The rims appear to be amorphous; no crystalline structure was noted even at a magnification of 220,000x. Also, XRD analyses show no evidence of a mineral of this composition. This amorphous material might be a film developed from the evaporation of sea spray. However, the lack of Cl is perplexing because one would think NaCl would be a precipitate. However, NaCl would not last long in a vadose meteoric environment. Another possibility is that the rims may be bacterial structures related to bacterial biofilms. Bacterial biofilms are well documented in marine fouling-release coating research (e.g., Dobretsov and Thomason, 2011; Mieszkin et al., 2012).

Stages of Cementation

The Cancún Eolianite shows a range of lithification. Figure 14 displays and summarizes these stages of increased diagenesis. These stages of diagenesis are similar to other Pleistocene and Holocene meteoric carbonate systems (Friedman, 1964; Land, 1969, 1970; Gavish and Friedman, 1969; Ward, 1975; Picha, 1978; Halley and Harris, 1979; Budd, 1988; Budd and Land, 1990). Stage 0 (Fig. 14A) is from within the dune but shows no



(FACING PAGE) Figure 10. Diagenesis of aragonite crystals. (A) Layer of pristine aragonite crystals. Other layers contain nanoballs. (B) Initial separation of aragonite crystals into nanoballs. (C) Abundant nanoballs and irregular aragonite crystals. (D) Predominance of nanoballs. (E) Stages of aragonite crystal transformation. (F) Possible calcite initiation and welding of crystals.

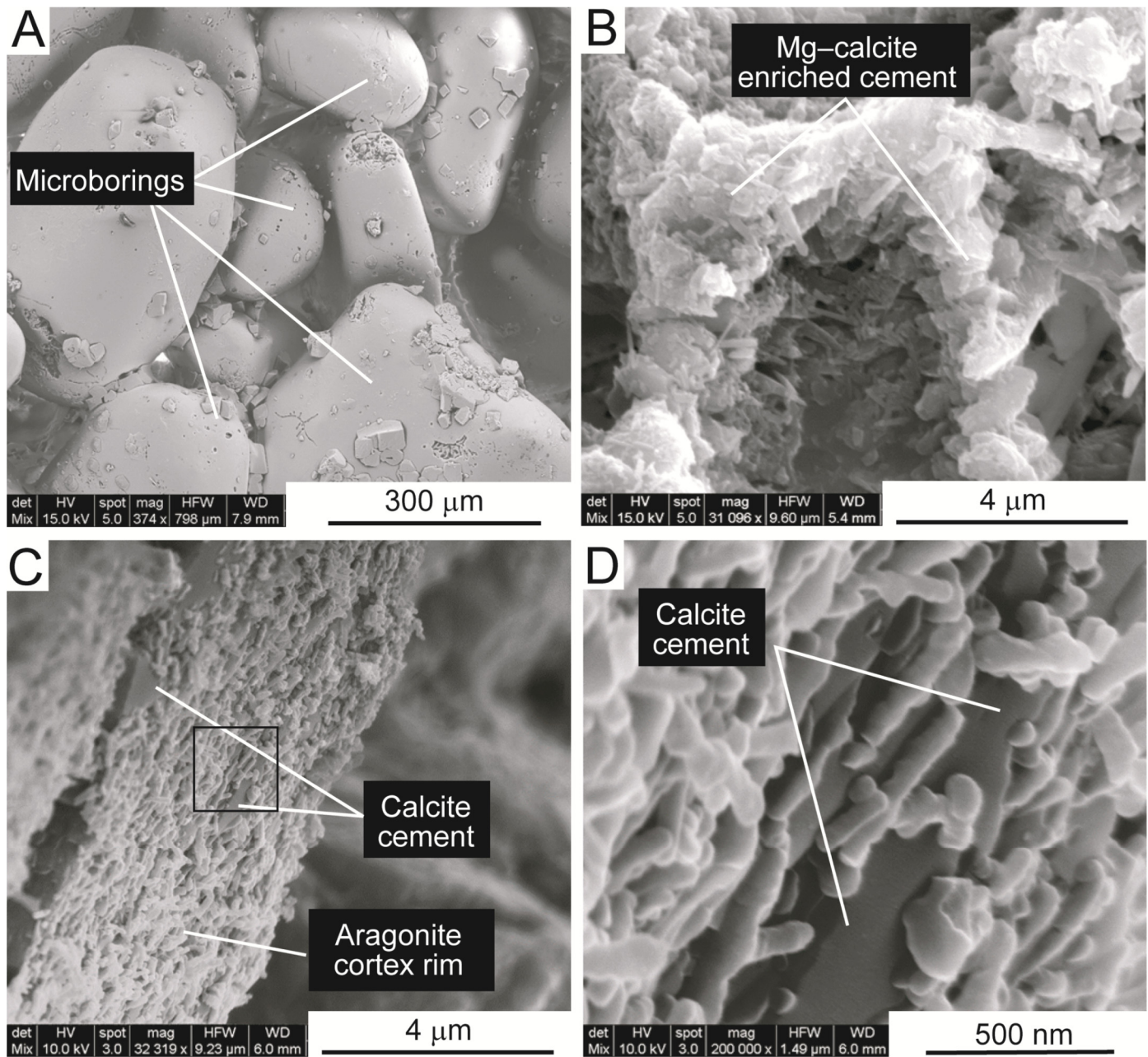
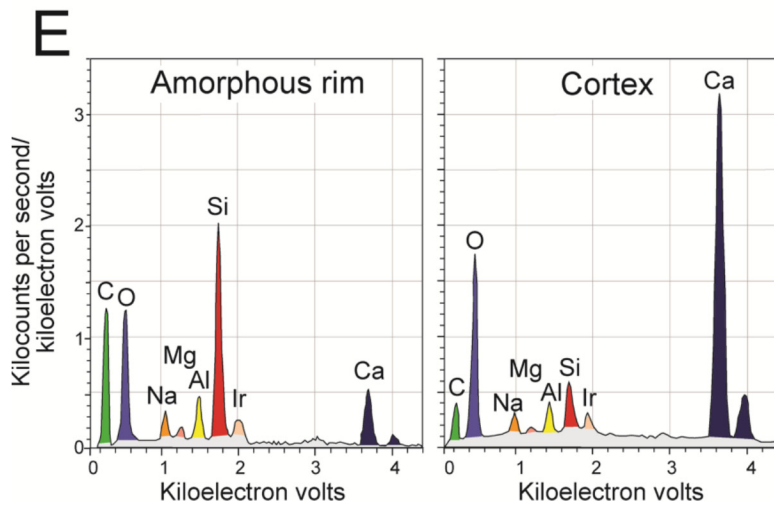
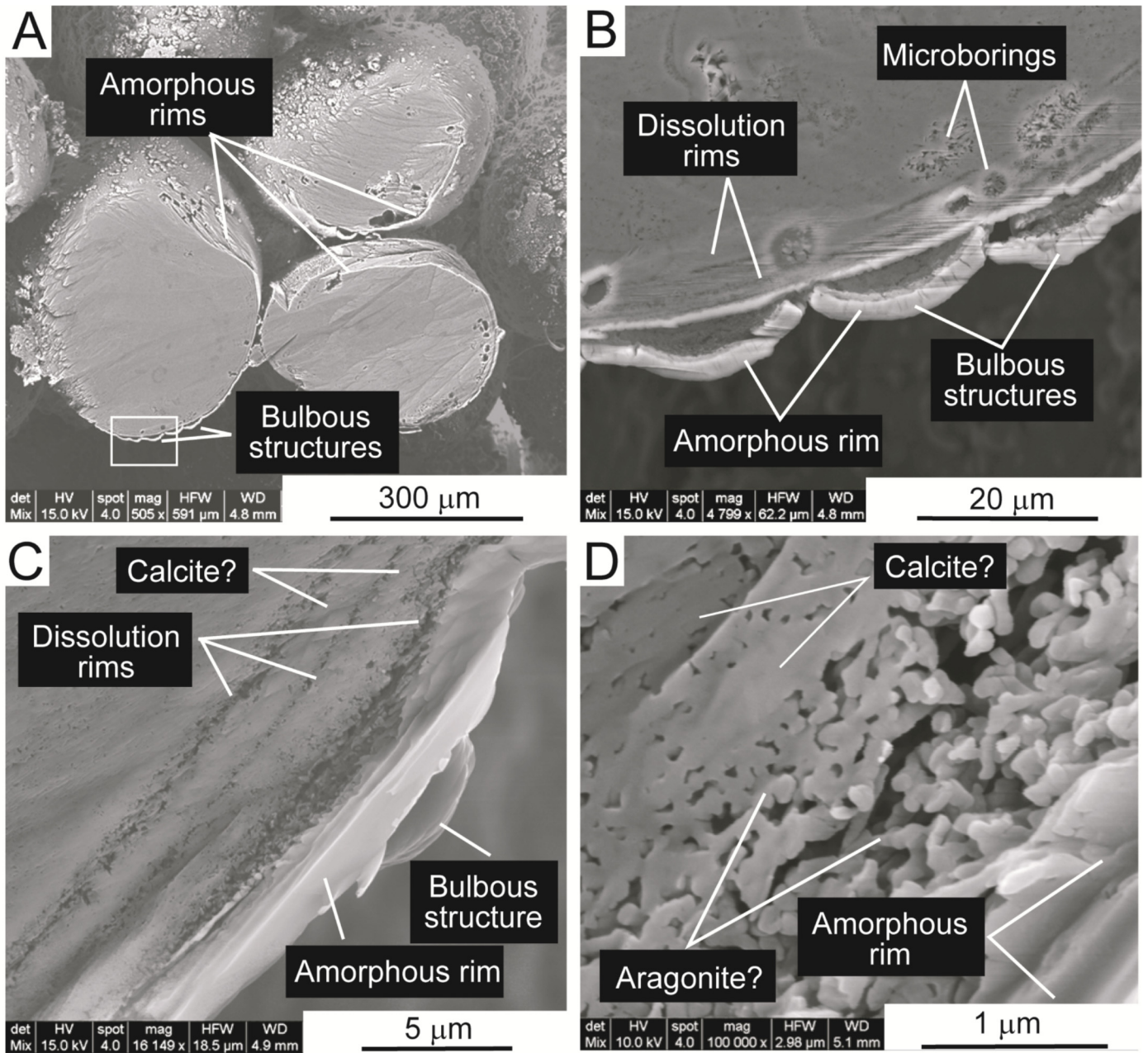


Figure 11. Cementation. (A) SEM image of ooids displaying microborings, meniscus cement, and grain-coating cement. (B) Mg-enriched aphanitic calcite cement precipitated around microboring. Mg enrichment was determined by EDS analysis on the FESEM. (C) Micron-sized calcite crystals embedded in aragonite crystals within ooid band. (D) Close-up of C showing the calcite crystal growing around and incorporating aragonite needles and nanoballs.

dissolution or cementation. The flow of vadose water must be bypassing this area, leaving the ooids unaltered. Stage 1 (Fig. 14B) displays incipient meniscus cementation between grains. Also, minor dissolution of ooid cortices is occurring in some of the ooids. Stage 2 (Fig. 14C) shows both meniscus cementation and ooid cortex dissolution increasing. A few interparticle pores are completely filled with equant calcite. Both *Halimeda* and *Goniolithon* nuclei are dissolving. Stage 3 (Fig. 14D) shows a

well-cemented ooid grainstone with few rounded interparticle pores, abundant oomoldic and concentric (in cortex) pores, and abundant micropores. Several of the incomplete cemented interparticle pores are rounded. The nuclei show a range of dissolution from grains appearing unaltered, to highly microporous grains, to moldic pores.

Figure 15 is a summary of major changes in mineralogy and porosity as diagenesis increases. The diagram is based on XRD



(FACING PAGE) Figure 12. Amorphous rims on ooids. All SEM images are from an Ar-ion milled sample. (A) Amorphous rims around three milled ooids appear as bright white lines. The bottom of the left ooid shows cross sections of bulbous structures. The bulbous structures are considered to be original but they also may have formed by separation from the grain during sample preparation. (B) Close-up of bulbous structures. Dissolution bands within the cortex are visible. Sample contains microborings with aragonite needles. (C) Close-up of rim shows an isolated bulbous structure. Rim shows no internal structure. Outer cortex of ooid shows several dissolution bands with remnant aragonite needles. Solid bands between the dissolution bands may be replacement calcite as the bands show no distinct aragonite crystals. (D) Close-up of dissolution band displaying altered aragonite needles and another band showing a possible layer of replacement calcite. (E) EDS spectrum contrasting elements in cortex and amorphous rim. Cortex is Ca rich and rim is Si rich.

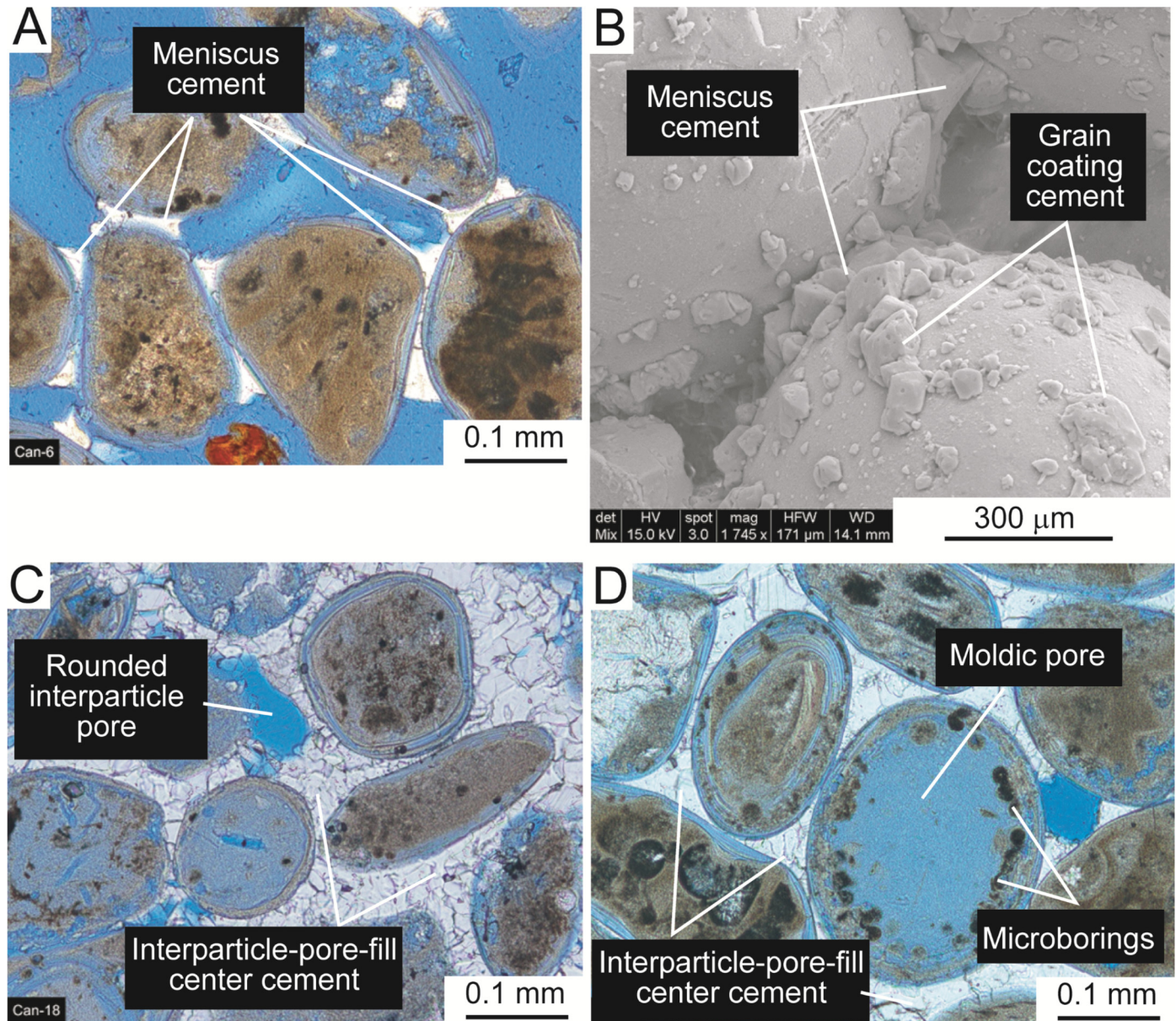


Figure 13. Cementation. (A) Meniscus cement. (B) SEM image of meniscus cement and grain-coating cement. (C) Interparticle pore-fill center cement. Ooid cortices have well-developed concentric dissolution bands. (D) Interparticle pore-fill center cement. Ooid cortices have well-developed concentric dissolution bands. Ooid grain in center has moldic pore outlined by mud-filled microborings. The dark mud in the microborings may be organic rich.

and thin-section analyses. Unstable Mg–calcite is totally dissolved as diagenesis advances, disappearing first because it is very unstable in meteoric water (Land, 1967) and not initially very abundant (<10%). Aragonite grains are still in the process of dissolving. The original calcite allochems are diagenetically stable, and their abundance remains constant. Vadose calcite cement increases from zero to an average of 20% as a result of aragonite and Mg–calcite dissolution. Primary porosity decreases

as the interparticle pores are cemented by calcite. Secondary dissolution pores consisting of moldic and micromoldic pores increase as aragonite and Mg–calcite allochems dissolve.

DISCUSSION

The investigation of the Cancun Eolianite provides data to address several important questions about carbonate diagenesis

and pore networks. The studied eolianite outcrop contains diagenetic features that are only a few thousands of years old or less. The oolitic sands also display varying degrees of diagenesis where the diagenetic fluid (meteoric water) is not in question. Therefore mineralogy, time, and diagenetic fluids are known constants.

Open Versus Closed Vadose Diagenetic System

With the abundant dissolution occurring in the Cancún Eolianite, it is important to understand where this recently dissolved calcium carbonate is transported and reprecipitated as a calcium-carbonate cement. The initial consideration is whether the vadose zone is an open or closed diagenetic system or if the calcium-carbonate-saturated waters percolate into the phreatic diagenetic zone below and precipitate as calcium-carbonate cement.

Figure 16A is a scatterplot based on thin-section point-count analysis of the amount of equant calcite vadose cement versus dissolution pores after aragonite and Mg-calcite allochems.

There is a strong positive correlation between calcite cement and dissolution of aragonite and Mg-calcite grains.

Despite the good correlation between grains dissolved and cement precipitated, the process is more complex than simple dissolution and reprecipitation. Aragonite has a higher density (2.93 g/cm^3) than calcite (2.71 g/cm^3); therefore, ideally, the dissolution of a given unit of aragonite will provide 1.08 units of calcite, an 8% increase. The percentage of Mg-calcite was so low (3–5%) that any volume change would be insignificant and not considered in the dissolution/reprecipitation process. Also, aragonite and Mg-calcite grains (*Halimeda* and *Goniolithon*) that dissolved were not solid but contained 10 to 20% micropores between the aragonite and Mg-calcite needles and rods. Point-count values of dissolved grains assumed that the dissolved grains were solid; therefore, a correction is needed in Figure 16A to account for these micropores and for the 8% volume increase produced relative to the density difference between aragonite and calcite.

The dashed line in Figure 16A shows the assumed correct relationship between grain dissolution and calcite precipitation if

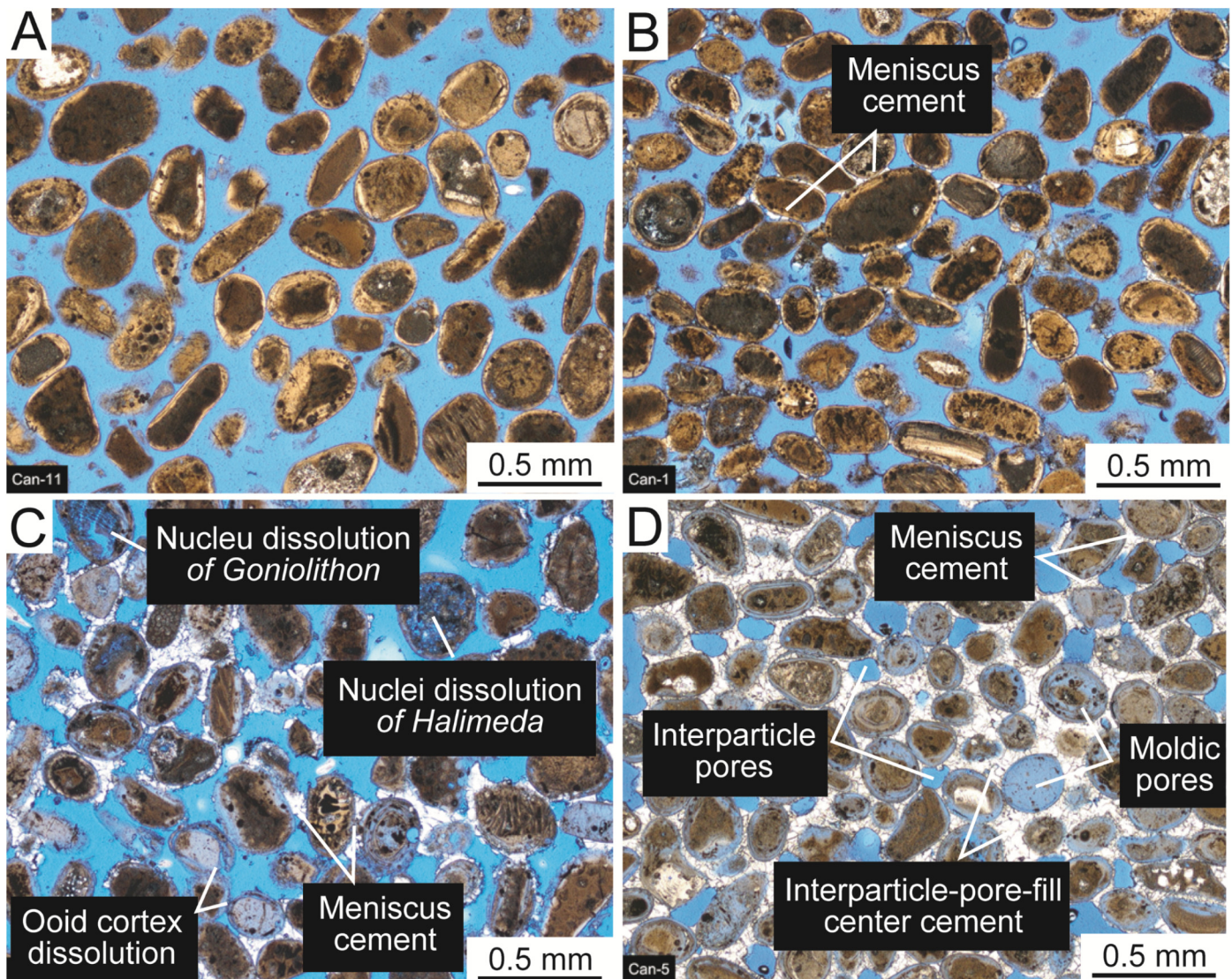


Figure 14. Stages of diagenesis. (A) Stage 0: No dissolution or cementation. (B) Stage 1: Incipient meniscus cementation between some grains. Also, minor dissolution of ooid cortices. (C) Stage 2: Increase of meniscus cementation and ooid cortex dissolution. A few interparticle pores are well cemented with equant calcite. Both *Halimeda* and *Goniolithon* nuclei display dissolution. (D) Stage 3: Well-cemented ooid grainstone with abundant moldic pores, cortex pores, and micropores. Several of the incomplete cemented interparticle pores are rounded. Nuclei show a range of dissolution from unaltered to highly microporous to moldic.

the system is closed. Many of the lower-value data points fall along the closed-system correlation line; however, many of the higher values are to the right of the line, indicating more calcite precipitated than can be accounted for by simple dissolution of the grains. The only possible source in these Holocene dunes would be dissolution of the dune surface. The upper dune surface in the eolianites is calichified, a product of dissolution and reprecipitation. Figure 16A suggests that some of the calcium carbonate dissolved at the surface of the dune flowed into the dune and added to calcite precipitation, thus accounting for the surplus of calcite cement. This discussion supports a closed system for the vadose zone because all the dissolved calcium carbonate can be accounted for and additional carbonate is acquired from calichification dissolution processes at the dune surface.

Another scattergram (Fig. 16B) of secondary intraparticle pores versus primary interparticle pores also shows a strong correlation, albeit negative, indicating that as secondary dissolution pores develop, primary interparticle pores are occluded. This negative relationship supports a relatively closed vadose system. From thin-section point-count calculations, pre-cement macroporosity (% primary pores + % interparticle pore cement) averages 34% after minor compaction of the whole rock, indicating that the amount of grains initially present should average 66% of the whole rock. The calculated amounts of grains currently present (% grains still present + % dissolution pores) is 62%, which is in close agreement with the predicted 66%, indicating a balance between dissolution of grains and cementation.

Formation of Oomoldic Pores without Cement

An interesting type of tight reservoirs in ancient carbonate systems is oomoldic-rich oolitic lime grainstones with abundant porosity and very marginal permeability, such as the Mid-East Permian Khuff ooid grainstone shown in Figure 17A. In this grainstone, the interparticle pores are filled with calcite cement, while the oomoldic pores are nearly cement free. What diagenetic processes occlude one pore type with cement, while leaving another pore type vacant? The Cancún Eolianite shows this process of differential cementation taking place.

This general diagenetic process is diagrammatically shown in Figure 18. The unstable aragonite and Mg–calcite nuclei are being dissolved, and the calcium carbonate being generated is

reprecipitated not within the newly formed pore but instead in the interparticle pores. There may be several causes for this phenomenon, but the one postulated by this study is that the newly forming oomoldic pores might be lacking calcite nucleation sites, whereas the interparticle pores may have available calcite nucleation sites such as the Mg–calcite cement rims around microborings (Figs. 11A and 11B), or the Mg–calcite micrite rims around the ooid produced by algae and fungi. Therefore, while dissolution is occurring, no cement can precipitate within the newly forming oomoldic pores.

Another observation is that some pores that at first glance appear to be oomoldic pores (material free) in thin section actually have a fine meshwork of remnant aragonite present (Figs. 8A, 13C, and 13D). In fact, oomoldic pores in an FESEM secondary electron image (Fig. 19A) show this remnant aragonite meshwork. Not until the complete ooid is dissolved can precipitation begin within the oomold, but, as noted above, there is a balance between grain dissolution and cement precipitation. Only if a new source of calcium carbonate is introduced into the system can the oomoldic pores become cemented.

Early Evolution of Pore Network in an Ooid Lime Grainstone

The Cancún Eolianite displays the early evolution of a pore network in an ooid-dominated grainstone. Original ooid sediment contained primary interparticle pores between ooids and abundant nano- and micropores within ooids (Figs. 3A and 14A). Initial depositional interparticle porosity in ooid sands was probably between 40 and 50% (Enos and Sawatsky, 1981), and porosity associated with micropores within the ooids could have added another 10 to 20% to the initial porosity. The ooids contain abundant nano- and micropores located between the aragonite and Mg–calcite needle and rods as revealed by FESEM imaging (Fig. 10). Porosity in the strata being cemented was measured by core-plug analysis. For these plugs to hold together, the strata had to be firm enough to be drilled. Therefore, the porosities measured by core-plug analysis are skewed to the better-cemented samples. Average porosity for the six plugs is 35.7%, with a range from 29.5 to 39.0%.

Pre-cement interparticle macroporosity of the Cancún Eolianite averages 34%, indicating that approximately six porosity

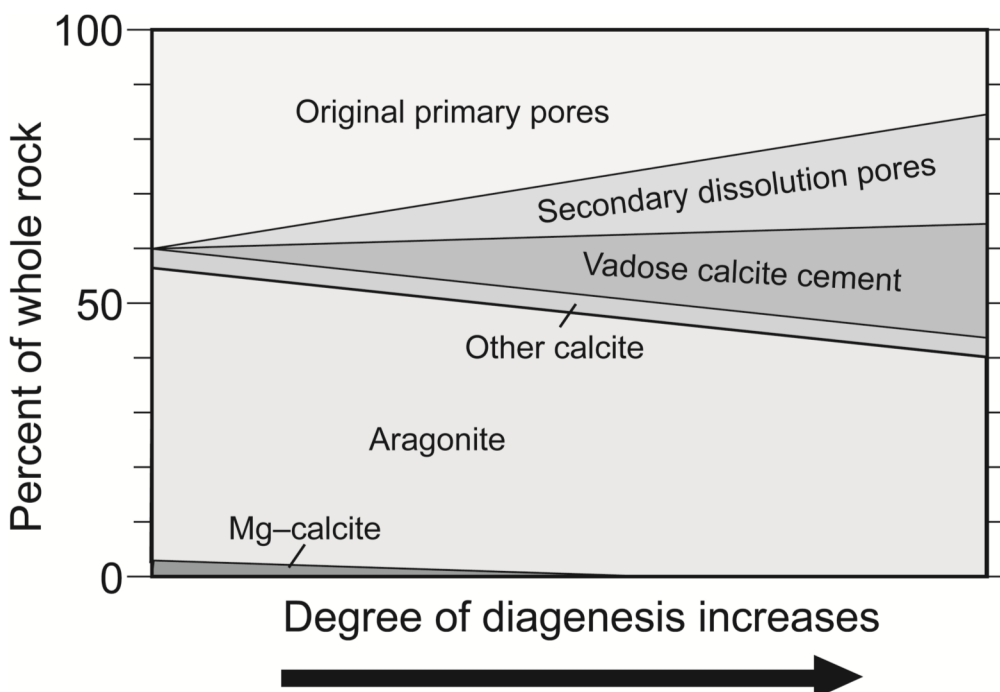


Figure 15. Summary of major changes in mineralogy and porosity as diagenesis advances.

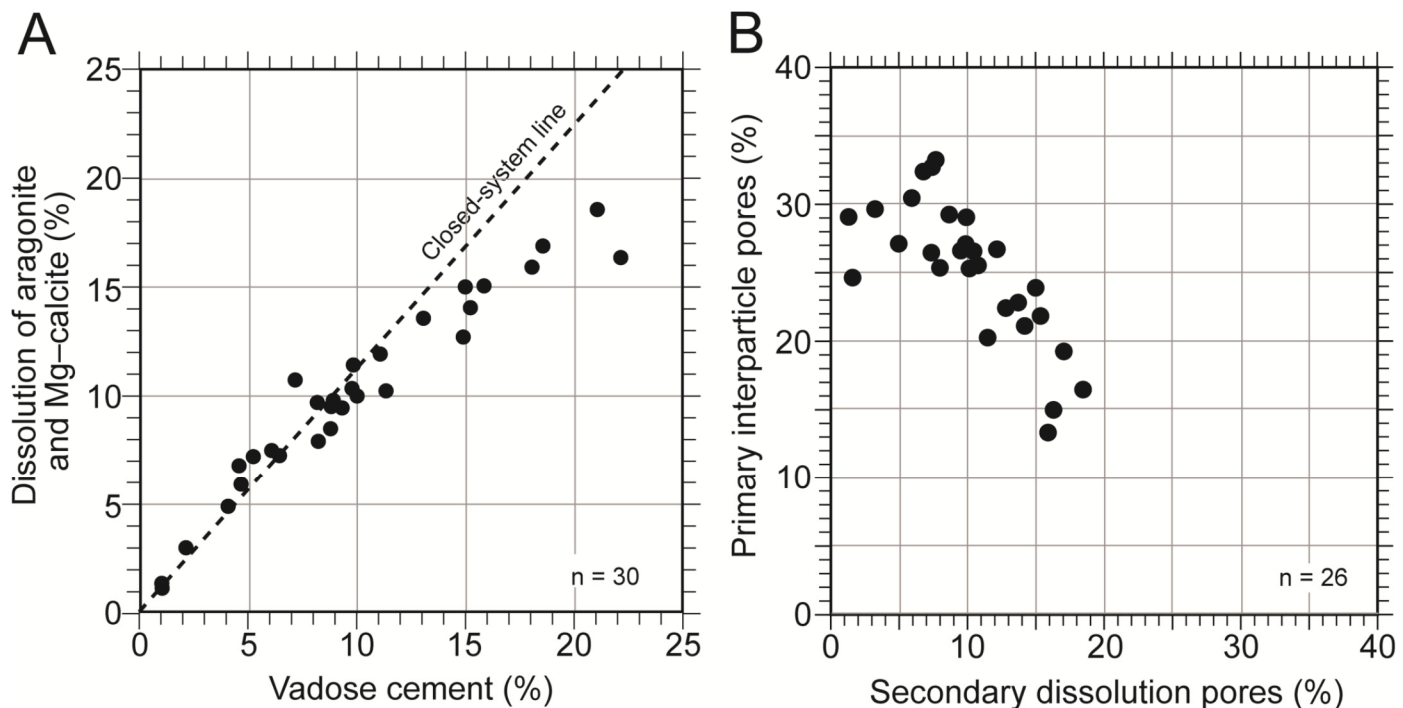


Figure 16. Mass-balance relationships. (A) Scattergram based on thin-section point-count analysis showing relationship between vadose cement and dissolution of aragonite and Mg-calcite. Dashed line shows ideal relationship between aragonite and Mg-calcite with 15% micropores (assumed average percent of micropores based on SEM analysis) versus calcite reprecipitation in a closed system. (B) Scattergram of the covariance of primary interparticle porosity and secondary dissolution porosity.

units or more were lost by compaction, assuming the initial sediment had 40% interparticle pores (Enos and Sawatsky, 1981) for the low end of initial porosity in carbonate spherical sands. It is interesting to see this much compaction within the dunes; we suggest that the weight of the dunes promoted minor, early compaction of the ooid sediments.

As diagenesis progressed, dissolution of the ooid nuclei created oomoldic pores, and the released calcium carbonate was reprecipitated in the interparticle pores, reducing the volume of the latter. The present macropore network after a few thousand years of diagenesis (Fig. 19) has produced a grainstone having an average of 24.3% (range = 14.7 to 32.9%) macroporosity. Nano- and micropores are estimated to be between 15 and 25%, based on the concept that thin-section point-count data provide percentage of macropores and that the difference between core-plug porosity and thin-section porosity provides percentage of micropores.

Pore casts were prepared for some of the samples and imaged using the FESEM (Figs. 19B–19D). The pore casts reveal the semi-3D view of the pore network. In Figs. 19B–19D, the areas of the nano- and micropores within the ooid cortex appear as continuous bands. The macropores are displayed as massive areas. The pore casts also emphasize the heterogeneity of the pore system (dual pore network) and the connectivity of the areas of different pores types.

With future burial of this ooid lime grainstone into the subsurface, several end-member pore-network scenarios could develop. One scenario would be a porous and permeable ooid grainstone where many of the interparticle pores are preserved. If micropores remained abundant in the ooids, the resulting pore network would be a dual-pore network. Another scenario is of a highly porous grainstone that has very low permeability because interparticle pores are completely occluded and oomoldic pores are abundant (Fig. 17A). A third scenario is that concentric band pores are abundant with or without interparticle and moldic pores (Figs. 17B–17D). Some excellent ancient examples of cortex-dissolution bands are presented by Cantrell (2006, his figures 5

and 6) and by Honarmand and Amini (2012, their figures 5B–5D). Without interparticle pores, concentric-band pores would produce a low-permeability reservoir because they may not be connected to the effective interparticle pore network. In actuality, any combination of these pores could develop during or survive burial down to 12,000 to 13,000 ft (3650 to 3950 m) without dolomitization (personal observation of senior author).

Carbonate-Eolian-Dune Preservation Potential

If other ancient carbonate-eolian dunes underwent relative rapid lithification similar to that of the Cancún Eolianite, their preservation potential would have been improved. The Cancún Eolianite—which has weathered many hurricanes, including Hurricane Gilbert in 1985—has been partly eroded but has the potential to persist far into the future. Loope and Abegg (2001) addressed the preservation of carbonate-eolian dunes and concluded that the dunes can be preserved into the subsurface, especially if they were originally aragonite rich. The aragonite-rich sediments would have supplied calcium carbonate to initiate early cementation and lithification. They noted that this early cementation may not happen in calcite-rich dunes.

Abegg et al. (2001) documented many carbonate paleoeolianites, which have the potential to be good hydrocarbon reservoirs because the grainstones can preserve abundant porosity and permeability if the interparticle pores are partly preserved and the volume of the eolianite is large. It is interesting to note that in modern environments, the thickest ooid deposits are not ooid shoals but rather oolitic eolianites, such as those seen in this investigation or on the eastern side of West Caicos Island and Long Beach on the southeast side of Providenciales in the Turks and Caicos. In these areas, ooid eolian dunes are up to 60 ft (18 m) high (Lloyd et al., 1987).

CONCLUSIONS

The Holocene Cancún Eolianite is an excellent natural laboratory for studying sedimentology, diagenesis, pore networks, and

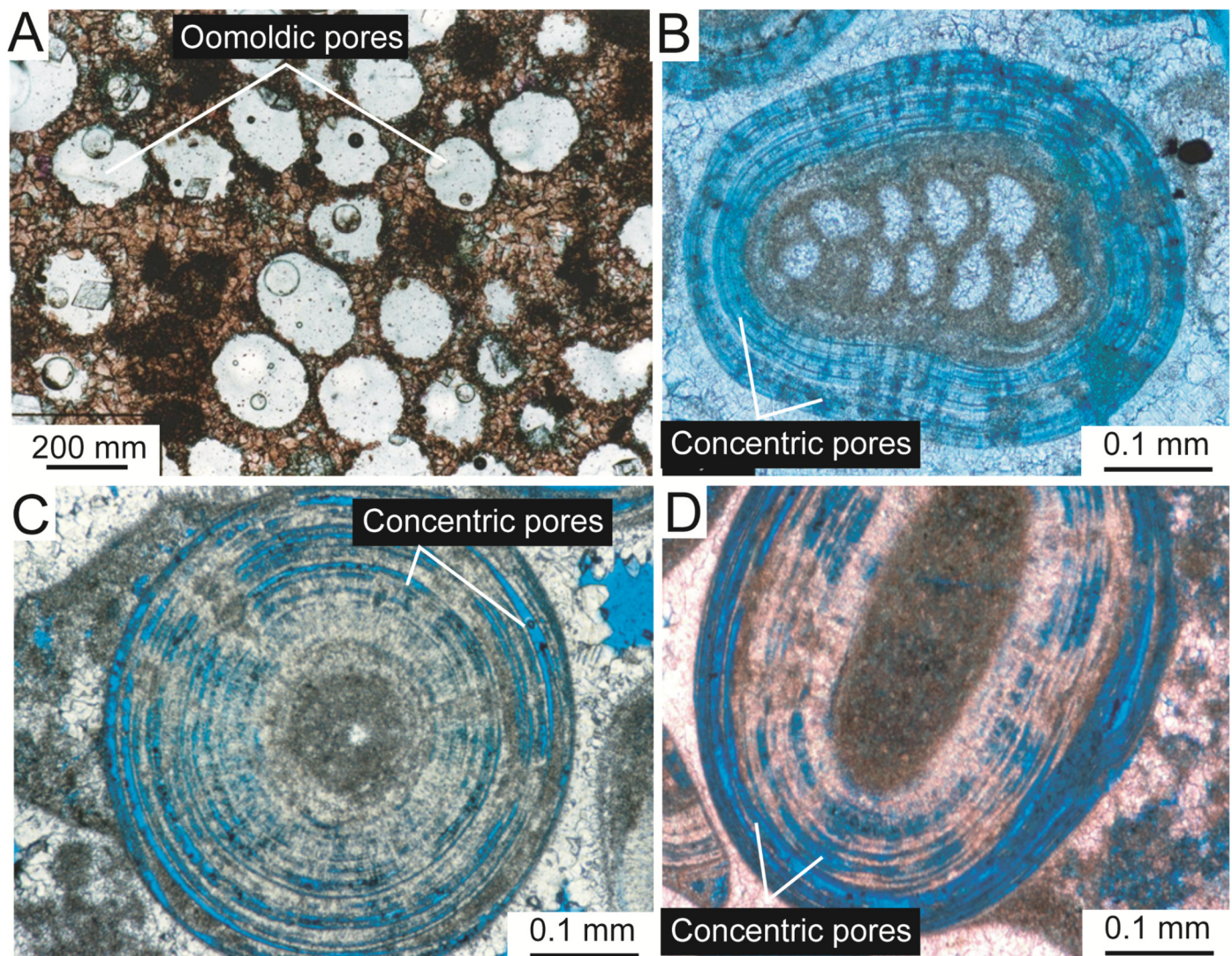


Figure 17. Pores in ancient ooid lime grainstones. (A) Permian-age Kluff ooid lime grainstone from the Mid-East with abundant oomoldic pores. Primary pore space is cemented tight. Calcite stained red. Porosity = 28% and permeability = 0.5 md. **(B)** Lower Cretaceous Glen Rose ooid lime grainstone from East Texas. Ooid cortex has bands of concentric dissolution similar to the Cancún Eolianite. **(C)** Mid-East Upper Jurassic Arab Formation ooid lime grainstone with well-developed concentric bands of pores. **(D)** Mid-East Upper Jurassic Arab Formation ooid lime grainstone with well-developed concentric bands of pores. Photomicrographs C and D are provided courtesy of Dave Cantrell.

the preservation potential of coastal carbonate-eolian dune systems. The eroded outcrop, comprised of loose ooid sand to lithified ooid grainstone, presents well-exposed dune stratification consisting of climbing translational stratification, grainfall laminations, and sandflow cross-stratification. The ooid allochems are predominantly aragonite, with lesser amounts of Mg–calcite and calcite. Because of the unstable mineralogy, advanced diagenesis is proceeding. Aragonite *Halimeda* and Mg–calcite *Goniolithon* ooid nuclei are dissolving to form oomoldic pores. In the aragonite cortices, the aragonite needles are dissolving by separating into nanoballs. The calcium carbonate generated by this dissolution is being precipitated as cement in the interparticle pore spaces and possibly in the ooid cortices. No cement is being reprecipitated in the dissolving nuclei. It is postulated that the lack of reprecipitation in the oomoldic pores is because the actively dissolving nuclei lack calcite nucleation sites. The Cancún Eolianite vadose zone acts as a relatively closed system with respect to the conservation of calcium carbonate. The amount of dissolution of aragonite and Mg–calcite approximates the amount of very fine- to fine-crystalline equant cement in the interparticle pore spaces. The early pore network has many similarities to ancient pore

networks in ooid grainstones, such as cement-reduced interparticle pores, oomoldic pores, concentric pores in cortices, and abundant nano- to micropores in the altered ooids. The concepts derived from investigating the Cancún Eolianite can be applied to understanding ancient ooid reservoirs and how their pore networks formed and evolved.

ACKNOWLEDGMENTS

The authors would like to express their appreciation to the reviewers of this manuscript (David Budd, Ling Gao, Peter Soto-Kerans, Mark Longman, and Peter Schemper); to Barry Katz, *GCAGS Journal* editor; to James J. Willis, *GCAGS* managing editor; and to Stephanie Jones, the Bureau of Economic Geology editor. Much of this work was accomplished at Atlantic Richfield Company (ARCO) and at the Bureau of Economic Geology Carbonate Reservoir Research Laboratory (RCRL). We thank Patrick Smith for working with us on the FESEM and aiding us in the production of the FESEM images. We recognize William Ward (now deceased) for his pioneering work on the sedimentology and diagenesis of carbonate systems using the Cancún Eo-

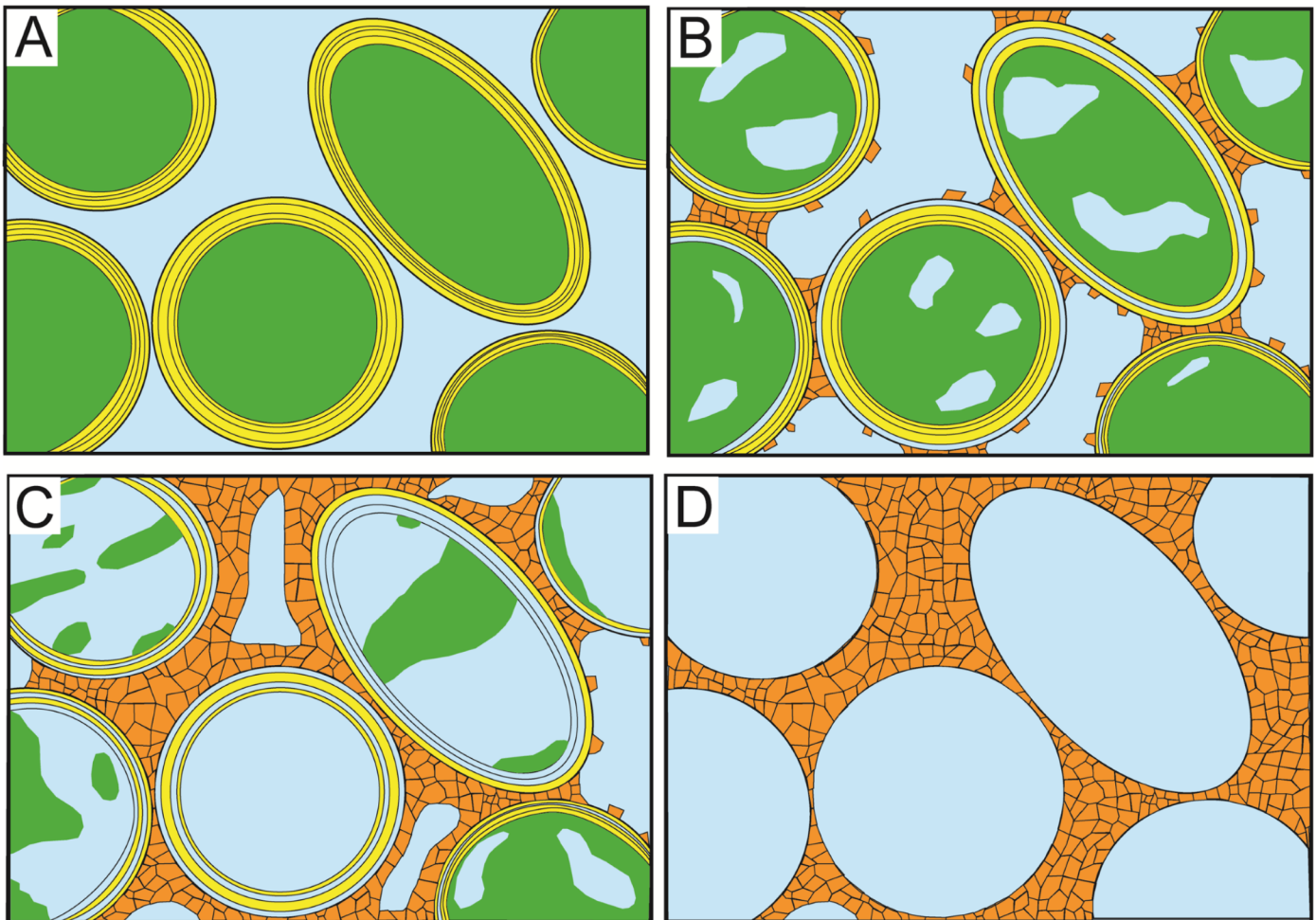


Figure 18. Schematic model for the development of a high-porosity, low-permeability oomoldic grainstone. (A) Unaltered ooid sand. (B) Early stage of Cancún Eolianite diagenesis. Initial dissolution of cortex rims and nuclei. Dissolved calcium carbonate is reprecipitated in interparticle pores. Dissolved nuclei are not chemically stable for precipitation of calcite. (C) Late stage of Cancún Eolianite diagenesis. Advanced cementation in interparticle pore spaces and intense dissolution of cortex rims and nuclei. All calcite precipitation is in interparticle pores because nuclei remain chemically unstable. (D) Future stage of diagenesis. Oomolds are free of cement and interparticle pores are nearly completely cemented. Molds remain open because all dissolved calcium carbonate was reprecipitated in interparticle pores. A new source of calcium carbonate would be needed to cement oomolds.

lianite. Publication authorized by the Director, Bureau of Economic Geology, Jackson School of Geosciences, University of Texas at Austin.

REFERENCES CITED

- Abegg, F. E., P. M. Harris, and D. B. Loope, eds., 2001, Modern and ancient carbonate eolianites: Sedimentology, sequence stratigraphy, and diagenesis: Society of Economic Paleontologists and Mineralogists (Society for Sedimentary Geology) Special Publication 71, Tulsa, Oklahoma, 207 p., doi:10.2110/pec.01.71.0017.
- Benson, D. J., and E. A. Mancini, 1982, Petrology and reservoir characteristics of the Smackover Formation, Hatter's Pond Field: Implications for Smackover exploration in southwestern Alabama: Gulf Coast Association of Geological Societies Transactions, v. 32, p. 67–75, doi:10.1306/03b5a7dc-16d1-11d7-8645000102c1865d.
- Budd, D. A., 1988, Petrographic products of freshwater diagenesis in Holocene ooid sands, Schooner Cays, Bahamas: Carbonates and Evaporites, v. 3, p. 143–163, doi:10.1007/bf03175114.
- Budd, D. A., and L. S. Land, 1990, Geochemical imprint of meteoric diagenesis in Holocene ooid sands, Schooner Cays, Bahamas: correlation of calcite geochemistry with extant groundwaters: Journal of Sedimentary Research, v. 60, p. 361–397, doi:10.1306/212f919c-2b24-11d7-8648000102c1865d.
- Budd, D. A., and E. M. Hiatt, 1993, Mineralogical stabilization of high-magnesium calcite: Geochemical evidence for intracrystal recrystallization within Holocene porcellaneous foraminifera: Journal of Sedimentary Research, v. 63, p. 261–374, doi:10.1306/d4267ad7-2b26-11d7-8648000102c1865d.
- Cantrell, D. L., 2006, Cortical fabrics of Upper Jurassic ooids, Arab Formation, Saudi Arabia: Implications for original carbonate mineralogy: Sedimentary Geology, v. 186, p. 157–170, doi:10.1016/j.sedgeo.2005.11.015.
- Clemmensen, L. B., and K. Abrahamsen, 1983, Aeolian stratification and facies association in desert sediments, Arran Basin (Permian), Scotland: Sedimentology, v. 30, p. 311–339, doi:10.1111/j.1365-3091.1983.tb00676.x.
- Current Results Publishing Ltd., 2017, Cancun temperatures & rainfall: Averages by month, <<http://www.currentresults.com/Weather/Mexico/Places/cancun-temperature-rainfall-averages-by-month.php>> Last accessed February 12, 2017.
- Dobretsov, S., and J. C. Thomason, 2011, The development of marine biofilms on two commercial non-biocidal coatings: A comparison between silicone and fluoropolymer technologies: Biofouling, v. 27, p. 869–880, doi:10.1080/08927014.2011.607233.
- Dunham, R. J., 1971, Meniscus cement, in O. P. Bricker, ed.,

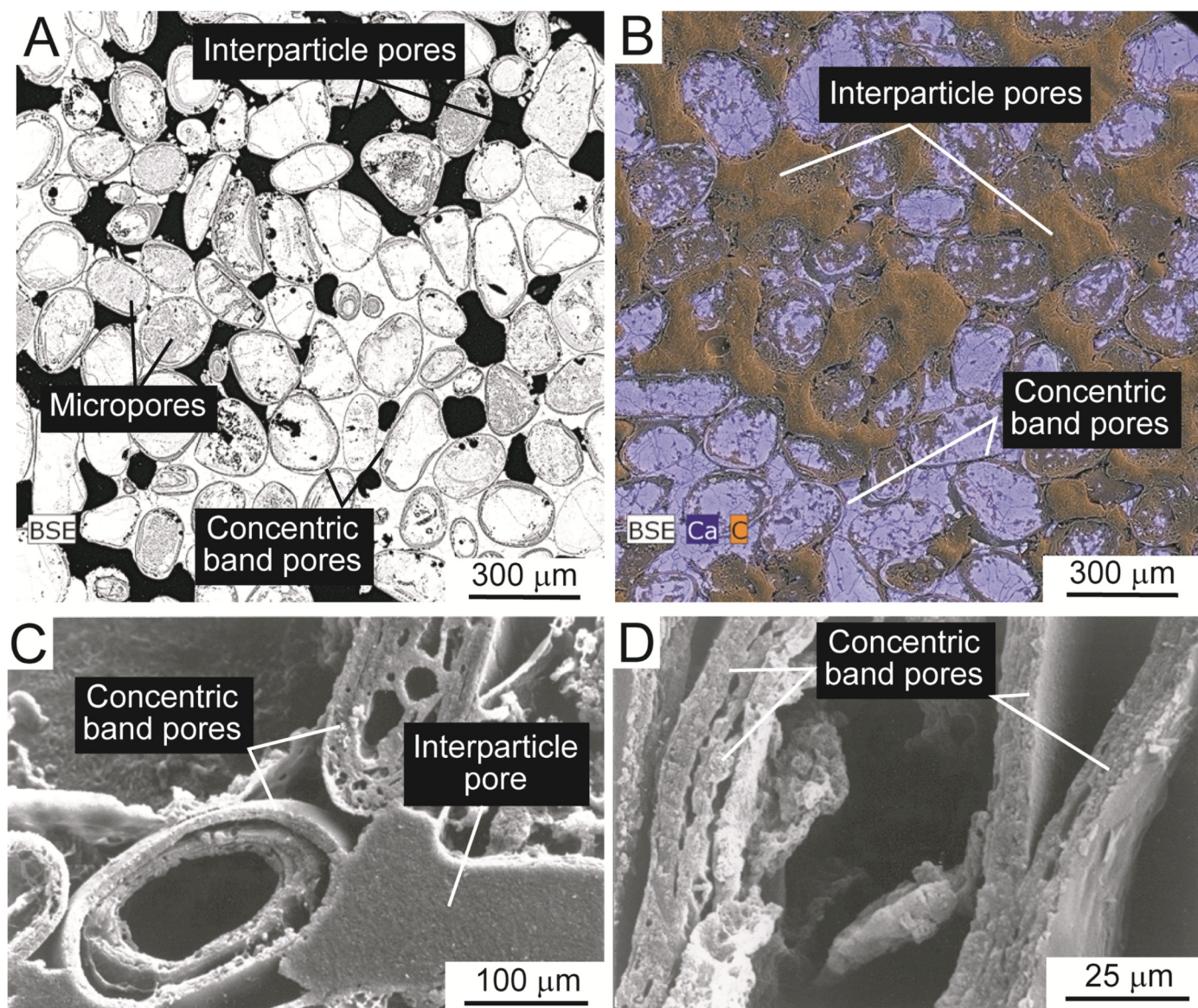


Figure 19. SEM-scale pore-network images. (A) High-contrast SEM image showing the pore network in black. **(B)** Pore network of a lightly cemented ooid grainstone. The porosity appears as orange brown. The aragonite appears as bluish gray. The display is a backscattered image overlain by an EDS map. Ca is a proxy for aragonite and C is a proxy for epoxy. Image shows a pore network of interparticle and concentric pores. **(C)** Secondary electron image of epoxy pore cast showing larger interparticle pores and concentric band pores. **(D)** Close-up of a secondary electron image of epoxy pore cast showing concentric band pores.

Carbonate cements: Johns Hopkins University Studies in Geology, Baltimore, Maryland, p. 297–300, doi:10.1017/s0016756800047439.

Enos, P., and L. H. Sawatsky, 1981, Pore networks in Holocene carbonate sediments: *Journal of Sedimentary Research*, v. 51, p. 961–985, doi:10.1306/212f7df1-2b24-11d7-8648000102c1865d.

Esfarili-Dizaji, B., and H. Rahimpour-Bonab, 2014, Generation and evolution of oolitic shoal reservoirs in the Permo-Triassic carbonates, the South Pars Field, Iran: *Facies*, v. 60, p. 921–940, doi:10.1007/s10347-014-0414-4.

Friedman, G. M., 1964, Early diagenesis and lithification in carbonate sediments: *Journal of Sedimentary Petrology*, v. 34, p. 777–813, doi:10.1306/74d71195-2b21-11d7-8648000102c1865d.

Fryberger, S. G., and S. Schenk, 1981, Wind sedimentation tunnel experiments on the origins of aeolian strata: *Sedimentology*, v. 28, p. 805–821, doi:10.1111/j.1365-3091.1981.tb01944.x.

Gavish, E., and G. M. Friedman, 1969, Progressive diagenesis in Quaternary to Late Tertiary carbonate sediments: Sequence and time scale: *Journal of Sedimentary Petrology*, v. 39, p. 980–1006, doi:10.1306/74d71d75-2b21-11d7-8648000102c1865d.

Harris, P. M., 1979, Facies anatomy and diagenesis of a Bahamian ooid shoal: University of Miami Comparative Sedimentology Laboratory, Sedimenta VII, Florida, 127 p. Available as American Association of Petroleum Geologists Search and Discovery Article 60022, Tulsa, Oklahoma, <http://www.searchanddiscovery.com/pdfz/documents/2009/60022_harris/harris.pdf.html> Last accessed June 12, 2017.

Halley, R. B., and P. M. Harris, 1979, Freshwater cementation of a 1000 year-old oolite: *Journal of Sedimentary Petrology*, v. 49, p. 969–988, doi:10.1306/212f7892-2b24-11d7-8648000102c1865d.

Honarmand, J., and A. Amini, 2012, Diagenetic processes and reservoir properties in the ooid grainstones of the Asmari Formation, Cheshmeh Khush Oil Field, SW Iran: *Journal of*

- Petroleum Science and Engineering, v. 81, p. 70–89, doi:10.1016/j.petrol.2011.12.022.
- Hover, V. C., L. M. Walter, and D. R. Peacor, 2001, Early marine diagenesis of biogenic aragonite and Mg–calcite: New constraints from high-resolution STEM and AEM analyses of modern platform carbonates: *Chemical Geology*, v. 175, p. 221–248, doi:10.1016/S0009-2541(00)00326-0.
- Hunter, R. E., 1977, Basic types of stratification in small eolian dunes: *Sedimentology*, v. 24, p. 361–387, doi:10.1111/j.1365-3091.1977.tb00128.x.
- Hunter, R. E., 1993, An eolian facies in the Ste. Genevieve Limestone of southern Indiana: Chapter 3, in B. D. Keith and C. W. Zuppang, eds., *Mississippian oolites and modern analogs: American Association of Petroleum Geologists Studies in Geology* 35, Tulsa, Oklahoma, p. 31–48.
- Keith, B. D., and E. D. Pittman, 1983, Bimodal porosity in oolitic reservoir—Effect on productivity and log response, Rodessa Limestone (Lower Cretaceous), East Texas Basin: *American Association of Petroleum Geologists Bulletin*, v. 67, p. 1391–1399, doi:10.1306/03b5ba2e-16d1-11d7-8645000102c1865d.
- Land, L. S., 1967, Diagenesis of skeletal carbonates: *Journal of Sedimentary Research*, v. 37, p. 914–930, doi:10.1306/74d717d5-2b21-11d7-8648000102c1865d.
- Land, L. S., 1970, Phreatic versus vadose meteoric diagenesis of limestones: Evidence from a fossil water table: *Sedimentology*, v. 14, p. 175–185, doi:10.1002/9781444304510.ch15.
- Lloyd, R. M., R. D. Perkins, and S. D. Kerr, 1987, Beach and shoreface ooid deposition on shallow interior banks, Turks and Caicos Islands, British West Indies: *Journal of Sedimentary Research*, v. 57, p. 976–982, doi:10.1306/212f8cbf-2b24-11d7-8648000102c1865d.
- Longman, M. W., T. G. Fertal, J. S. Glennie, C. G. Krazan, D. H. Suck, W. G. Toler, and K. S. Wiman, 1983, Description of a paraconformity between carbonate grainstones, Isla Cancún, Mexico: *Journal of Sedimentary Research*, v. 53, p. 533–542, doi:10.1306/212f8224-2b24-11d7-8648000102c1865d.
- Loope, D. B., and F. E. Abegg, 2001, Recognition and geologic preservation of ancient carbonate eolianites, in F. E. Abegg, P. M. Harris, and D. B. Loope, eds., *Modern and ancient carbonate eolianites: Sedimentology, sequence stratigraphy, and diagenesis: Society of Economic Paleontologists and Mineralogists (Society for Sedimentary Geology) Special Publication 71*, Tulsa, Oklahoma, p. 3–16, doi:10.2110/pec.01.71.0003.
- Loucks, R. G., and W. C. Ward, 2001, Stratification and beach-to-dune transition in a Holocene carbonate eolianite complex, Isla Cancún, Quintana Roo, Mexico, in F. E. Abegg, P. M. Harris, and D. B. Loope, eds., *Modern and ancient carbonate eolianites: Sedimentology, sequence stratigraphy, and diagenesis: Society of Economic Paleontologists and Mineralogists (Society for Sedimentary Geology) Special Publication 71*, Tulsa, Oklahoma, p. 57–76, doi:10.2110/pec.01.71.0057.
- Loucks, R. G., R. M. Reed, S. C. Ruppel, and D. M. Jarvie, 2009, Morphology, genesis, and distribution of nanometer-scale pores in siliceous mudstones of the Mississippian Barnett Shale: *Journal of Sedimentary Research*, v. 79, p. 848–861, doi:10.2110/jsr.2009.092.
- Loucks, R. G., F. J. Lucia, and L. E. Waite, 2013, Origin and description of the micropore network within the Lower Cretaceous Stuart City Trend tight-gas limestone reservoir in Pawnee Field in South Texas: *Gulf Coast Association of Geological Societies Journal*, v. 2, p. 29–41, <<http://www.gcags.org/Journal/2013.GCAGS.Journal/GCAGS.Journal.2013.vol2.p29-41.Loucks.et.al.pdf>> Last accessed June 14, 2017.
- Macintyre, I. G., and R. P. Reid, 1998, Recrystallization in living porcelaneous foraminifera (*Archaias angulatis*): Textural changes without mineralogic alternation: *Journal of Sedimentary Research*, v. 68, p. 11–19, doi:10.2110/jsr.68.11.
- McLaren, S., 1995, The role of sea spray in vadose diagenesis in late Quaternary coastal deposits: *Journal of Coastal Research*, v. 11, p. 1075–1088, <<https://www.jstor.org/stable/4298412>> Last accessed June 14, 2017.
- McLaren, S., and E. Gardner, 2000, New radiocarbon dates from a Holocene aeolinite, Isla Cancún, Quintana Roo, Mexico: *The Holocene*, v. 10, p. 757–761, doi:10.1191/09596830095006.
- McLaren, S., and E. Gardner, 2004, Late Quaternary vadose carbonate diagenesis in coastal and desert dune and beach sands: Is that a palaeoclimatic signal?: *Earth Surface Processes and Landforms*, v. 29, p. 1441–1458, doi:10.1002/esp.1132.
- Matthews, R. K., 1967, Diagenetic fabrics in biosparites from the Pleistocene of Barbados, West Indies: *Journal of Sedimentary Petrology*, v. 37, p. 1147–1153, doi:10.1306/74d71852-2b21-11d7-8648000102c1865d.
- Matthews, R. K., 1968, Carbonate diagenesis: Equilibrium of sedimentary mineralogy to the subaerial environment; Coral Cap of Barbados, West Indies: *Journal of Sedimentary Petrology*, v. 38, p. 1110–1119, doi:10.1306/74d71b13-2b21-11d7-8648000102c1865d.
- Mieszkin, S., P. Martin-Tanchereau, M. E. Callow, and J. A. Callow, 2012, Effect of bacterial biofilms formed on fouling-release coatings from natural seawater and *Cobetia marina*, on the adhesion of two marine algae: *Biofouling*, v. 28, p. 953–968, doi:10.1080/08927014.2012.723696.
- Picha, F., 1978, Depositional and diagenetic history of Pleistocene and Holocene oolitic sediments and sabkhas in Kuwait, Persian Gulf: *Sedimentology*, v. 25, p. 427–450, doi:10.1111/j.1365-3091.1978.tb00320.x.
- Steinen, R. P., and R. K. Matthews, 1973, Phreatic vs. vadose diagenesis: Stratigraphy and mineralogy of a cored borehole on Barbados, W.I.: *Journal of Sedimentary Petrology*, v. 43, p. 1012–1020, doi:10.1306/74d728d8-2b21-11d7-8648000102c1865d.
- Strasser, A., and E. Davaud, 1986, Formation of Holocene limestone sequences by progradation, cementation, and erosion: Two examples from the Bahamas: *Journal of Sedimentary Geology*, v. 56, p. 422–428, doi:10.1306/212f8936-2b24-11d7-8648000102c1865d.
- Ward, W. C., 1975, Petrology and diagenesis of carbonate eolianites of northeastern Yucatán Peninsula, Mexico, in K. F. Wantland and W. C. Pusey, eds., *Belize shelf-carbonate sediments, clastic sediment, and ecology: American Association of Petroleum Geologists Studies in Geology* 2, Tulsa, Oklahoma, p. 500–571.
- Ward, W. C., 1997, Geology of coastal islands, northeastern Yucatán Peninsula, in H. L. Vacher and T. M. Quinn, eds., *Geology and hydrogeology of carbonate islands: Developments in Sedimentology*, v. 54, p. 275–298, doi:10.1016/S0070-4571(04)80029-3.
- Ward, W. E., and M. J. Brady, 1979, Strandline sedimentation of carbonate grainstones, upper Pleistocene, Yucatán Peninsula, Mexico: *American Association of Petroleum Geologists Bulletin*, v. 63, p. 362–369, doi:10.1306/clea5616-16c9-11d7-8645000102c1865d.
- Winland, H. D., 1968, The role of high Mg calcite in the preservation of micrite envelopes and textural features of aragonite sediments: *Journal of Sedimentary Research*, v. 38, p. 1320–1325, doi:10.1306/74d71b6d-2b21-11d7-8648000102c1865d.